HOLTEC INTERNATIONAL

Holtec Center, 555 Lincoln Drive West, Marlton, NJ 08053
Telephone (609) 797-0900
Fax (609) 797-0909

LICENSING REPORT

for

SPENT FUEL RACK INSTALLATION

at

BYRON AND BRAIDWOOD NUCLEAR STATIONS

Holtec Report HI-982083 (Non-Proprietary Version)
Report Category: A

Prepared for Commonwealth Edison Co.
Purchase Order No. 367585
Holtec Project 80944

HOLTEC INTERNATIONAL

Holtec Center, 555 Lincoln Drive West, Marlton, NJ 08053
Telephone (609) 797- 090
Fax (609) 797 - 090

REVIEW AND CERTIFICATION LOG

DOCUMENT NAME	LICENSING REPORT FOR BYRON/BRAIDWOOD NUCLEAR STATIONS
HOLTEC DOCUMENT I.D. NUMBER	982083
HOLTEC PROJECT NUMBER	80944
CUSTOMER/CLIENT:	COMMONWEALTH EDISON

REVISION BLOCK

REVISION NUMBER *	AUTHOR & DATE !!	REVIEWER & DATE !!	QA & DATE !!	APPROVED & DATE !	DIST. X
ORIGINAL					
REVISION 1					
REVISION 2					
REVISION 3					
REVISION 4					
REVISION 5					
REVISION 6	Carl W. Burkhardt C. Burkhardt 9/29/99	Rita Chadhay RCC 9/29/99	M DHDD 9/29/99	Carl W. Burkhardt C. Burkhardt 9/29/99	C

SEE PREVIOUS REVIEW & CERT. LOG

!! This document conforms to the requirements of the design specification and the applicable sections of the governing codes.By signing on this page, you are confirming that you have filled out the DVC questionnaire stored in Holtec's network directory n:\pdoxwin\working\dvc.

Note : Signatures and printed names required in the review block.

* A revision of this document will be ordered by the Project Manager and carried out if any of its contents is materially affected during evolution of this project. The determination as to the need for revision will be made by the Project Manager with input from others, as deemed necessary by

! Must be Project Manager or his designee

x Distribution : C : Client
M : Designated Manufacturer
F : Florida Office

*** Report category on the cover page indicates the contractual status of this document as ***
A = to be submitted to client for approval I = for client's information N = not submitted externally

THE REVISION CONTROL OF THIS DOCUMENT IS BY A "SUMMARY OF REVISIONS LOG" PLACED BEFORE THE TEXT OF THE REPORT.

SUMMARY OF REVISIONS

Revision 0: Inititial issue.

Revision 1: Figures 11.1 through 11.13, which showed a preliminary rack change-out sequence, were removed from Chapter 11 (Installation) and the List of Figures. Minor corrections were also made to the Table of Contents.

Revision 2: Text was added to Sections 11.5 and 11.6, which describe the fuel shuffling and the new rack installation. Minor changes were also made to the Table of Contents.

Revision 3: Minor changes were made to Paragraph 11.1 h. (ALARA Procedure), Subsection 11.7.2, and Subsection 11.7.3.

Revision 4: Editorial changes were made on pages 1-1, 5-2, 5-17, 8-7, and 8-11.

Revision 5: Chapter 7 was reorganized to include a section on construction accidents (i.e., rack drop accident). Figure 6.5.1 and Table 8.2 were also corrected. Table 6.5.3 was added to the report. These changes also affected the Table of Contents and the List of Figures.

Revision 6: A new paragraph was added to Section 6.4 (Synthetic Time Histories) on page 6-6. Minor editorial changes were also made on pages 6-12 and 6-14.

6.0 STRUCTURAL SEISMIC CONSIDERATIONS

6.1 Introduction

This chapter considers the structural adequacy of the new maximum density spent fuel racks under all loads postulated for normal, seismic, and accident conditions at Byron and Braidwood Nuclear stations.

As discussed in Chapter 1, the reracking of the Byron and Braidwood pools involves replacement of existing high-density storage racks with new racks with a slight increase in the total capacity. The reracking is being undertaken to remove the Boraflex neutron material from the two pools because of its ongoing degradation and loss in neutron attenuation ability. The new racks, like the existing racks, will be installed in a free-standing configuration. At the time of the previous rerack, however, the state-of-the-art limited the seismic evaluation to single rack 3-D simulations. As we discuss in this chapter, it is now possible to model the entire assemblage of rack modules in one comprehensive simulation known as the 3-D Whole Pool Multi-Rack (WPMR) analysis. In order to maintain continuity with the previous analysis methods, both single rack and WPMR analyses have been performed to establish the structural margins of safety in the Byron/Braidwood racks.

The analyses undertaken to confirm the structural integrity of the racks are in full compliance with the USNRC Standard Review Plan [6.1.1] and the OT Position Paper [6.1.2]. For each of the analyses, an abstract of the methodology, modeling assumptions, key results, and summary of parametric evaluations are presented. Delineation of the relevant criteria are discussed in the text associated with each analysis.

6.2 Overview of Rack Structural Analysis Methodology

The response of a free-standing rack module to seismic inputs is highly nonlinear and involves a complex combination of motions (sliding, rocking, twisting, and turning), resulting in impacts and friction effects. Some of the unique attributes of the rack dynamic behavior include a large fraction of the total structural mass in a confined rattling motion, friction support of rack pedestals against lateral motion, and large fluid coupling effects due to deep submergence and motion of closely spaced prismatic structures.

Linear methods, such as modal analysis and response spectrum techniques, cannot accurately simulate the structural response of such a highly nonlinear structure to seismic excitation. An accurate simulation is obtained only by direct integration of the nonlinear equations of motion with the three pool slab acceleration time-histories applied as the forcing functions acting simultaneously.

Both Whole Pool Multi-Rack (WPMR) and Single Rack (SR) analysis are used in this project to simulate the dynamic behavior of the high density rack structures described in Chapter 2 of this report. The following sections provide the basis for the selection of the appropriate methodology and discussion on its development.

6.2.1 Background of Analysis Methodology

Reliable assessment of the stress field and kinematic behavior of the rack modules calls for a conservative dynamic model incorporating all *key attributes* of the actual structure. This means that the model must feature the ability to execute the concurrent motion forms compatible with the free-standing configuration of the modules.

The model must possess the capability to effect momentum transfers which occur due to rattling of fuel assemblies inside storage cells and the capability to simulate lift-off and subsequent impact of support pedestals with the pool liner (or bearing pad). The contribution of the water mass in the interstitial spaces around the rack modules and within the storage cells must be modeled in an accurate manner since erring in quantification of fluid coupling on either side of the actual value is no guarantee of conservatism.

The Coulomb friction coefficient at the pedestal-to-pool liner (or bearing pad) interface may lie in a rather wide range and a conservative value of friction cannot be prescribed *a priori*. In fact, a perusal of results of rack dynamic analyses in numerous dockets (Table 6.2.1) indicates that an upper bound value of the coefficient of friction often maximizes the computed rack displacements as well as the equivalent elastostatic stresses.

In short, there are a large number of parameters with potential influence on the rack kinematics. The comprehensive structural evaluation must deal with all of these without sacrificing conservatism.

The three-dimensional single rack dynamic model introduced by Holtec International personnel in the Enrico Fermi Unit 2 rack project (ca. 1980) and used in some 50 rerack projects since that time, including Byron and Braidwood in the late 80s (Table 6.2.1) addresses most of the above mentioned array of parameters. The details of this methodology are also published in the permanent literature [6.2.1]. Despite the versatility of the 3-D seismic model, the accuracy of the single rack simulations has been suspect due to one key element; namely, hydrodynamic participation of water around the racks. During dynamic rack motion, hydraulic energy is either drawn from or added to the moving rack, modifying its submerged motion in a significant manner. Therefore, the dynamics of one rack affects the motion of all others in the pool.

However, Single Rack analysis is still a valuable tool to examine the behavior of a rack under different load conditions. It is used here as a first step in evaluating the racks. WPMR analysis builds upon the Single Rack model. The worst-case loads and stresses that result from these two models are used to determine the structural adequacy of the racks.

The 3-D rack model dynamic simulation, involving one or more spent fuel racks, handles the array of variables as follows:

Interface Coefficient of Friction Parametric runs are made with upper bound and lower bound values of the coefficient of friction (COF). The limiting values are based on experimental data that have been found to be bounded by the values 0.2 and 0.8. Simulations are also performed with the array of pedestals having randomly chosen coefficients of friction in a Gaussian distribution with a mean of 0.5 and lower and upper limits of 0.2 and 0.8, respectively. In the fuel rack simulations, the Coulomb friction interface between rack support pedestal and liner is simulated by piecewise linear (friction) elements. These elements function only when the pedestal is physically in contact with the pool liner.

Rack Elastic Behavior Rack elasticity, relative to the rack base, is included in the model by introducing linear springs to represent the elastic bending action, twisting, and extensions.

Impact Phenomena Compression-only gap elements are used to provide for opening and closing of interfaces such as the pedestal-to-bearing pad interface, and the fuel assembly-to-cell wall interface. These interface gaps are modeled using nonlinear spring elements. The term "nonlinear spring" is a generic term used to denote the mathematical representation of the condition where a restoring force is not linearly proportional to displacement.

Fuel Loading Scenarios The fuel assemblies are conservatively assumed to rattle in unison, which obviously exaggerates the effect of fuel impacts against the cell walls. Partial fuel loadings (e.g., a rack that has fuel assemblies in only half of its cells) are simulated by offsetting the center of gravity of the stored fuel mass with respect to the rack center of gravity, as appropriate.

Fluid Coupling Holtec International extended Fritz's classical two-body fluid coupling model to multiple bodies and utilized it to perform the first two-dimensional multi-rack analysis (Diablo Canyon, ca. 1987). Subsequently, laboratory experiments were conducted to validate the multi-rack fluid coupling theory. This technology was incorporated in the computer code DYNARACK [6.2.4] which handles simultaneous simulation of all racks in the pool as a Whole Pool Multi-Rack 3-D analysis. This development was first utilized in Chinshan, Oyster Creek, and Shearon Harris plants in the 80's [6.2.1, 6.2.3] and, subsequently, in numerous other rerack projects. The WPMR analyses have corroborated the accuracy of the single rack 3-D solutions in predicting the maximum structural stresses, and also serve to improve predictions of rack kinematics.

The Whole Pool Multi-Rack (WPMR) model used to predict the dynamic behavior of the storage racks contains elements specifically designed to represent the attributes necessary to simulate rack motions during earthquakes. These elements include non-linear springs to develop the interaction between racks, between racks and walls, and between fuel assemblies and rack internal cell walls. Hydrodynamic effects within these interstitial spaces are accounted for using Fritz's classical method which relates the fluid kinetic energy in the annulus due to relative motion to an equivalent hydrodynamic mass.

The modeling technique used was chosen based on the applicable Codes, Standards and Specifications given in Section IV (2) of the NRC guidance on spent fuel pool modifications entitled, "Review and Acceptance of Spent Fuel Storage and Handling Applications," dated April 14, 1978, which states that "Design...may be performed based upon the AISC specification or Subsection NF requirements of Section III of the ASME B&PV Code for Class 3 component supports." The rack modeling technique is consistent with the linear support beam-element type members covered by these codes.

Although it is acknowledged that finite element models could be developed using plate and fluid elements which may also provide satisfactory simulated behavior for a single rack, there is no known commercial finite element code which can treat multi-body fluid interaction correctly and sufficiently account for near and far field fluid effects involving many bodies (racks) in a closed pool. It is for this reason that the global dynamic analysis uses the formulation specifically developed and contained within DYNARACK.

The computer software validation of the DYNARACK program is documented in validation manual HI-91700. The validation manual demonstrates that the DYNARACK code verification is adequate for engineering applications without further experimental verification.

For closely spaced racks, demonstration of kinematic compliance is verified by including all modules in one comprehensive simulation using a WPMR model. In WPMR analysis, all rack modules are modeled simultaneously and the coupling effect due to this multi-body motion is included in the analysis. Due to the superiority of this technique in predicting the dynamic behavior of closely spaced submerged storage racks, the Whole Pool Multi-Rack analysis methodology is used as the principal vehicle for seismic qualification in the Byron/Braidwood project.

6.3 Description of Racks and Fuel

As discussed in Chapter 3, the proposed rack layouts for Byron and Braidwood are identical. A total of twenty-four racks is proposed to be installed in each pool. Four new racks use a flux-trap design and are referred to as Region I racks. The remaining racks do not utilize flux-traps and are referred to as Region II racks. The dynamic rack models include all twenty-four racks. For dynamic simulations, the dry fuel weight is conservatively taken to be 1600 lbs.

6.4 Synthetic Time-Histories

Synthetic time-histories in three orthogonal directions (N-S, E-W, and vertical) are generated in accordance with the provisions of SRP 3.7.1 [6.4.1]. In order to prepare an acceptable set of acceleration time-histories, Holtec International's proprietary code GENEQ [6.4.2] is utilized.

A preferred criterion for the synthetic time-histories in SRP 3.7.1 calls for both the response spectrum and the power spectral density (PSD) corresponding to the generated acceleration time-

history to envelope their target (design basis) counterparts with only finite enveloping infractions. The time-histories for the pools have been generated to satisfy this preferred (and more rigorous) criterion.

The design response spectra used to develop the synthetic time histories is the envelope of the Byron spectra and Braidwood spectra obtained from the building seismic models at the fuel pool elevation. This is believed to be conservative because the Byron foundation is on rock whereas the Braidwood foundation is comprised of soil. Furthermore, the broadened design spectra of the envelope curves are used to make the comparison with the response spectra of the synthetic time histories.

The target PSD is generated using a program called GENEQ. GENEQ is a Q.A. validated synthetic time-history generator and has been used by Holtec International to generate statistically independent artificial acceleration time histories in over 40 reracking projects. GENEQ accepts an initial digitized response spectra as input and generates a new bounding response spectra along with a PSD corresponding to both the target and generated spectra along with an acceleration time history.

To prepare the PSD, the digitized design basis response spectra for the elevation of interest (at the floor of the pool) was initially input to obtain the target response spectra and target PSD and a generated spectra and PSD. If the generated spectra and PSD does not bound the initially input target, then an iterative process begins which involves revising the input spectra (by broadening, increasing peak values, etc.) to establish a bounding spectra and PSD. At the completion of each iterative step the newly generated spectra and PSD are compared against the target spectra and PSD developed from the initially input digitzed design basis response spectra. If necessary, the response spectra data is smoothed to prepare comparable results.

The synthetic time-histories in the three directions also satisfy the requirements of statistical independence mandated by SRP 3.7.1.

Figures 6.4.1 through 6.4.3 and 6.4.4 through 6.4.6 provide plots of the time-history accelerograms that were generated over a 20-second duration for SSE and OBE events, respectively. These artificial time-histories are used in all non-linear dynamic simulations of the racks.

Results of the correlation function of the three time-histories are given in Table 6.4.1. It is noted that the absolute values of all correlation coefficients are well below 0.15 indicating that the desired statistical independence of the three data sets has been met.

6.5 3-D Nonlinear Rack Model for Dynamic Analysis

6.5.1 General Remarks

The single rack 3-D model of the Byron/Braidwood racks has been prepared with due consideration of the following characteristics, which are typical of high-density modules designed by Holtec International.

i. As a continuous structure, the rack possesses an infinite number of degrees-of-freedom (DOF), of which the cantilever beam type modes are most pronounced under seismic excitation if the rack is of the honeycomb construction genré. (The Byron/Braidwood racks, like all prior Holtec designs, are of the honeycomb type.)

ii. The fuel assemblies are "nimble" structures with a relatively low beam mode fundamental frequency.

iii. The interstitial gap between the storage cells and the stored fuel assemblies leads to a rattling condition in the storage cells during a seismic event.

iv. The lateral motion of the rack due to seismic input is resisted by the pedestal-to-pool slab interfacial friction and is abetted or retarded by the fluid coupling forces produced by the proximity of the rack to other structures. (The fluid coupling forces are distinct from the nonconservative forces such as fluid "drag" which are, by NRC regulations, excluded from the analysis). The construction of a 3-D single rack dynamic model consists of modeling the rack as a multi-degree-of-freedom structure in such a manner that the selected DOFs capture all macro-motion modes of the rack, such as twisting, overturning, lift-off, sliding, flexing, and combinations thereof. Particular attention must be paid to incorporating the potential for the friction-resisted sliding of the rack on the liner, lift-off and subsequent impact of the pedestals on the slab, collision of the rack with adjacent structures, and most important, rattling of the fuel in the storage cells. The

dynamic model must also provide for the ability to simulate the scenarios of partially loaded racks with arbitrary loading patterns.

As the name implies, the Single Rack (SR) dynamic model is a 3-D structural model for *one* rack in the pool. The rack selected for the SR analysis in this project is the one with the most mass, or most non-square cross section (i.e., pool aspect ratio). The dynamic model of this rack, i.e., its structural stiffness characteristics, rattling effect of the stored fuel, etc., can be prepared with extreme diligence in the manner described in the following, resulting in an excellent articulation of the rack structure. Even the fluid coupling effects between the fuel assemblies and the storage cell can be modeled with acceptable accuracy [6.5.2]. If the rack is adjacent to a wall, the fluid coupling effects between the rack and the wall can also be set down deterministically because the wall is a fixed structure. Such a definitive situation does not exist, however, when the neighboring structure to the subject rack is another free-standing rack. During a seismic event, the subject rack and the neighboring rack will both undergo dynamic motions which will be governed by the interaction among the inertia, fluid, friction, and rattling forces for each rack. The fluid coupling forces between two racks, however, depend on their *relative* motions. Because the motion of the neighboring rack is undefined, it is not possible to characterize the hydrodynamic forces arising from the fluid coupling between the neighboring rack and the subject rack. This inability to accurately model the inter-rack fluid coupling effects is a central limitation in the single rack analysis.

To overcome this limitation intrinsic to the single rack solutions, an artificial boundary condition, referred to as the "out-of-phase" assumption, has been historically made to bound the problem.

In the out-of-phase assumption, it is assumed that *all* racks adjacent to the subject rack are vibrating 180° out-of-phase, resulting in a plane of symmetry between the subject rack and the neighboring rack, across which water will not flow. Thus, the subject rack is essentially surrounded by a fictitious box with walls that are midway to the adjacent racks. Impact with the adjacent rack is assumed to have occurred if the subject rack contacts the "box wall".

In summary, in the out-of-phase motion analysis the analyst makes the election that the adjacent racks are moving at 180° out-of-phase from the subject rack at all times during the seismic event. This is an artificial technical construct, albeit one that is known to predict rack-to-rack impact conservatively.

However, this assumption also increases the relative contribution of fluid coupling, which depends on fluid gaps and relative movements of bodies, making overall conservatism a less certain assertion. As is well known, the fluid forces between adjacent rack modules can reach rather large values in closely spaced rack geometries. It is, therefore, essential that the contribution of the fluid forces be included in a comprehensive manner. This is possible only if all racks in the pool are *allowed* to execute 3-D motion in the mathematical model. For this reason single rack, or even multi-rack models involving only a portion of the racks in the pool, are inherently inaccurate. The Whole Pool Multi-Rack model removes this intrinsic limitation of the rack dynamic models by simulating the 3-D motion of all modules simultaneously. The fluid coupling effect, therefore, encompasses interaction between *every* set of racks in the pool, i.e., the motion of one rack produces fluid forces on all other racks and on the pool walls. Stated more formally, both near-field and far-field fluid coupling effects are included in the WPMR analysis.

Therefore, to maintain consistency with past analyses, an array of single rack 3-D simulations were carried out, principally to compare the results (viz., rack-to-rack impact, maximum primary stress levels, pedestal loads, etc.) with the more definitive WPMR analysis. The description below provides the essentials of the 22 DOF model for a single rack. This model is used in both 3-D single rack simulations and as the building block for the more complicated WPMR analyses, which are described later in this chapter.

The dynamic modeling of the rack structure is prepared with special consideration of all nonlinearities and parametric variations. Particulars of modeling details and assumptions for the rack analysis are given in the following:

a. The fuel rack structure motion is captured by modeling the rack as a 12 degree-of-freedom structure. Movement of the rack cross-section at any height is described by six degrees-of-freedom of the rack base and six degrees-of-freedom at the rack top. In this manner, the response of the module, relative to the baseplate, is captured in the dynamic analyses once suitable springs are introduced to couple the rack degrees-of-freedom and simulate rack stiffness.

b. Rattling fuel assemblies within the rack are modeled by five lumped masses located at H, .75H, .5H, .25H, and at the rack base (H is the rack height measured above the baseplate). Each lumped fuel mass has two horizontal displacement degrees-of-freedom. Vertical motion of the fuel assembly mass is assumed equal to rack vertical motion at the baseplate level. The centroid of each fuel assembly mass can be located off-center, relative to the rack structure centroid at that level, to simulate a partially loaded rack.

c. Seismic motion of a fuel rack is characterized by random rattling of fuel assemblies in their individual storage locations. An upper bound on the effective cumulative fuel assembly mass is established using the previously described artificial time histories.

d. Fluid coupling between rack and fuel assemblies, and between rack and wall, is simulated by appropriate inertial coupling in the system kinetic energy. Inclusion of these effects uses the methods of [6.5.2, 6.5.3] for rack/assembly coupling and for rack-to-rack coupling.

e. Fluid damping and form drag are conservatively neglected.

f. Sloshing is found to be negligible at the top of the rack and is, therefore, neglected in the analysis of the rack.

g. Potential impacts between the cell walls of the new racks and the contained fuel assemblies are accounted for by appropriate compression-only gap elements between masses involved. The possible incidence of rack-to-wall or rack-to-rack impact is simulated by gap elements at the top and bottom of the rack in two horizontal directions. Bottom gap elements are located at the baseplate elevation. The initial gaps reflect the presence of baseplate extensions, and the rack stiffnesses are chosen to simulate local structural detail.

h. Pedestals are modeled by gap elements in the vertical direction and as "rigid links" for transferring horizontal stress. Each pedestal support is mathematically linked to the pool liner (or bearing pad) by two friction springs. The spring rate for the friction springs includes any lateral elasticity of the stub pedestals. Local pedestal vertical spring stiffness accounts for floor elasticity and for local rack elasticity just above the pedestal.

i. Rattling of fuel assemblies inside the storage locations causes the gap between fuel assemblies and cell wall to change from a maximum of twice the nominal gap to a theoretical zero gap. Fluid coupling coefficients are based on the nominal gap in order to provide a conservative measure of fluid resistance to gap closure.

j. The model for the rack is considered supported, at the base level, on four pedestals modeled as non-linear compression only gap spring elements and eight piecewise linear friction spring elements; these elements are properly located with respect to the centerline of the rack beam, and allow for arbitrary rocking and sliding motions.

6.5.2 Element Details

Figure 6.5.1 shows a schematic of the dynamic model of a single rack. The schematic depicts many of the characteristics of the model including all of the degrees-of-freedom and some of the spring restraint elements.

Table 6.5.1 provides a complete listing of each of the 22 degrees-of-freedom for a rack model. Six transitional and six rotational degrees-of-freedom (three of each type on each end) describe the motion of the rack structure. Rattling fuel mass motions (shown at nodes 1^*, 2^*, 3^*, 4^*, and 5^* in Figure 6.5.1) are described by ten horizontal transitional degrees-of-freedom (two at each of the five fuel masses). The vertical fuel mass motion is assumed (and modeled) to be the same as that of the rack baseplate.

Figure 6.5.2 depicts the fuel to rack impact springs (used to develop potential impact loads between the fuel assembly mass and rack cell inner walls) in a schematic isometric. Only one of the five fuel masses is shown in this figure. Four compression only springs, acting in the horizontal direction, are provided at each fuel mass. Figure 6.5.3 provides a 2-D schematic elevation of the storage rack model, discussed in more detail in Section 6.5.3. This view shows the vertical location of the five storage masses and some of the support pedestal spring members.

Figure 6.5.4 shows the modeling technique and degrees-of-freedom associated with rack elasticity. In each bending plane a shear and bending spring simulate elastic effects [6.5.4]. Linear elastic springs coupling rack vertical and torsional degrees-of-freedom are also illustrated in this figure.

Figure 6.5.5 depicts the inter-rack impact springs (used to develop potential impact loads between racks or between rack and wall). The approximate spring contact location and numbering of each impact spring used in the model are shown in Figure 6.8.1 and Figure 6.8.2.

6.5.3 Fluid Coupling Effect

In its simplest form, the so-called "fluid coupling effect" [6.5.2, 6.5.3] can be explained by considering the proximate motion of two bodies under water. If one body (mass m_1) vibrates adjacent to a second body (mass m_2), and both bodies are submerged in frictionless fluid, then Newton's equations of motion for the two bodies are:

$$(m_1 + M_{11})\,X_1 + M_{12}\,X_2 = \text{applied forces on mass } m_1 + O(X_1^2)$$

$$M_{21}\,X_1 + (m_2 + M_{22})\,X_2 = \text{applied forces on mass } m_2 + O(X_2^2)$$

X_1 and X_2 denote absolute accelerations of masses m_1 and m_2, respectively, and the notation $O(X^2)$ denotes nonlinear terms. The hydrodynamic coupling effect is shown to be composed of an added nonlinear term which varies with geometry and a component which varies with the square of velocity. This is easily shown by considering a typical example where fluid coupling plays a significant role. Consider two long beams of length "l" width "h" and a distance "s" apart:

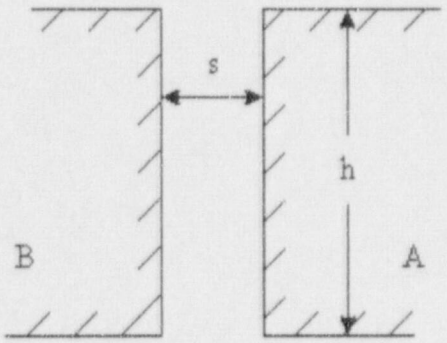

It is assumed that s<<h<<l which is always the case for spent fuel racks. It is shown by Levy [6.6.1] that the force exerted by the fluid on "beam" A is given by

$$F_{opening} = \frac{\rho l h^3}{12 s}\left(-\ddot{s} - \frac{\dot{s}^2}{2s}\right) \qquad \text{(A moves to the right)}$$

$$F_{opening} = \frac{\rho l h^3}{12 s}\left(-\ddot{s} + \frac{\dot{s}^2}{s}\right) \qquad \text{(A moves to the left)}$$

The above solution is valid at each instant in time so that as the beams (racks) approach each other larger forces result which tend to reduce rack motion and preclude rack-to-rack impact. For conservative results, the rack analyses are based only on the nominal gap that exists prior to any seismic event. Therefore the forces exerted have the form.

$$F = C\left(-s \pm \alpha s^2\right)$$

The non-linear term for the case of a prismatic fuel assembly in a square cell has been derived by Soler & Singh (1982). "Dynamic Coupling in a Closely Spaced Two-Body System Vibrating in Liquid Medium: The Case of Fuel Racks".

In the actual spent fuel rack analyses, the geometry is more complex but the resulting non-linearities have the same character of an added mass multiplier by the acceleration of the rack plus a velocity squared fluid damping term. As the interstitial gap changes, the resulting fluid mass changes also result in non-linear terms. The non-linear terms, O (X_1^2) and O (X_2^2), been consistently neglected in order to maintain the requirement that no credit be taken for fluid damping in the seismic analysis.

M_{11}, M_{12}, M_{21}, and M_{22} are fluid coupling coefficients which depend on body shape, relative disposition, etc. Fritz [6.5.3] gives data for M_{ij} for various body shapes and arrangements. The fluid adds mass to the body (M_{11} to mass m_1), and an inertial force proportional to acceleration of the adjacent body (mass m_2). Thus, acceleration of one body affects the force field on another. This force field is a function of inter-body gap, reaching large values for small gaps. Lateral motion of a fuel assembly inside a storage location encounters this effect. For example, fluid coupling behavior will be experienced between nodes 2 and 2* in Figure 6.5.1. The rack analysis also contains inertial fluid coupling terms that model the effect of fluid in the gaps between adjacent racks.

These terms are usually computed assuming that all racks adjacent to the rack being analyzed are vibrating in-phase or 180 degrees out of phase. The WPMR analyses do not require any assumptions with regard to phase.

Rack-to-rack gap elements have initial gaps set to 100% of the physical gap between the racks or between outermost racks and the adjacent pool walls.

6.5.4 Stiffness Element Details

Table 6.5.2 lists all spring elements used in the 3-D 22-DOF single rack model. It helps to explain the stiffness details. Byron and Braidwood are mirror images about the E-W direction.

The analysis for Braidwood serves for Byron as well. In the table, the following coordinate system applies:

x = Horizontal axis along Braidwood plant North (Byron, South)
y = Horizontal axis along Braidwood plant West (Byron, East)
z = Vertical axis upward from the rack base

If the simulation model is restricted to two dimensions (one horizontal motion plus one vertical motion, for example), for the purposes of model clarification only, then Figure 6.5.3 describes the configuration. This simpler model is used to elaborate on the various stiffness modeling elements.

Type 3 gap elements modeling impacts between fuel assemblies and racks have local stiffness K_i in Figure 6.5.3. In Table 6.5.2, for example, type 3 gap elements 5 through 8 act on the rattling fuel mass at the rack top. Support pedestal spring rates K_S are modeled by type 3 gap elements 1 through 4, as listed in Table 6.5.2. Local compliance of the concrete floor is included in K_S. The type 2 friction elements listed in Table 6.5.2 are shown in Figure 6.5.3 as K_f. The spring elements depicted in Figure 6.5.4 represent type 1 elements.

Friction at support/liner interface is modeled by the piecewise linear friction springs with suitably large stiffness K_f up to the limiting lateral load μN, where N is the current compression load at the interface between support and liner. At every time-step during transient analysis, the current value of N (either zero if the pedestal has lifted off the liner, or a compressive finite value) is computed.

The gap element K_S, modeling the effective compression stiffness of the structure in the vicinity of the support, includes stiffness of the pedestal, local stiffness of the underlying pool slab, and local stiffness of the rack cellular structure above the pedestal.

The previous discussion is limited to a 2-D model solely for simplicity. Actual analyses incorporate 3-D motions and include all stiffness elements listed in Table 6.5.2. Table 6.5.3 provides a list of typical stiffness values, which are used to model the spent fuel racks for Byron and Braidwood.

6.6 Whole Pool Multi-Rack Methodology

6.6.1 General Remarks

The single rack 3-D (22-DOF) models for the new racks outlined in the preceding subsection are used as a first step to evaluate the structural integrity and physical stability of the rack modules. However, prescribing the motion of the racks adjacent to the module being analyzed is an assumption in the single rack simulations that cannot be defended on the grounds of conservatism. For closely spaced racks, demonstration of the kinematic compliance is further verified by including all modules in one comprehensive simulation using a Whole Pool Multi-Rack (WPMR) model. The WPMR analysis builds on the Single Rack model by simultaneously modeling all racks with full consideration of the multi-body fluid coupling effects (discussed in the next subsection).

Recognizing that the analysis work effort must deal with both stress and displacement criteria, the sequence of model development and analysis steps that are undertaken are summarized in the following:

a. Prepare 3-D dynamic models suitable for a time-history analysis of the new maximum density racks. These models include the assemblage of all rack modules in the pool. Include all fluid coupling interactions and mechanical coupling appropriate to performing an accurate non-linear simulation. This 3-D simulation is referred to as a Whole Pool Multi-Rack model.

b. Perform 3-D dynamic analyses on various physical conditions (such as coefficient of friction and extent of cells containing fuel assemblies). Archive appropriate displacement and load outputs from the dynamic model for post-processing.

c. Perform stress analysis of high stress areas for the limiting case of all rack dynamic analyses. Demonstrate compliance with ASME Code Section III, Subsection NF limits on stress and displacement.

6.6.2 Multi-Body Fluid Coupling Phenomena

During the seismic event, all racks in the pool are subject to the input excitation simultaneously. The motion of each free-standing module would be autonomous and independent of others as long as they do not impact each other and no water is present in the pool. While the scenario of

inter-rack impact is not a common occurrence and depends on rack spacing, the effect of water – the so-called fluid coupling effect – is a universal factor. As noted in Ref. [6.5.2, 6.5.3], the fluid forces can reach rather large values in closely spaced rack geometries. It is, therefore, essential that the contribution of the fluid forces be included in a comprehensive manner. This is possible only if all racks in the pool are *allowed* to execute 3-D motion in the mathematical model. For this reason, single rack or even multi-rack models involving only a portion of the racks in the pool, are inherently inaccurate. The Whole Pool Multi-Rack model removes this intrinsic limitation of the rack dynamic models by simulating the 3-D motion of all modules simultaneously. The fluid coupling effect, therefore, encompasses interaction between *every* set of racks in the pool, i.e., the motion of one rack produces fluid forces on all other racks and on the pool walls. Stated more formally, both near-field and far-field fluid coupling effects are included in the analysis.

The derivation of the fluid coupling matrix [6.6.2] relies on the classical inviscid fluid mechanics principles, namely the principle of continuity and Kelvin's recirculation theorem. While the derivation of the fluid coupling matrix is based on no artificial construct, it has been nevertheless verified by an extensive set of shake table experiments [6.6.2].

6.6.3 Coefficients of Friction

To eliminate the last significant element of uncertainty in rack dynamic analyses, multiple simulations are performed to adjust the friction coefficient ascribed to the support pedestal/pool bearing pad interface. These friction coefficients are chosen consistent with the two bounding extremes from Rabinowicz's data [6.5.1]. Simulations are also performed by imposing intermediate value friction coefficients developed by a random number generator with Gaussian normal distribution characteristics. The assigned values are then held constant during the entire simulation in order to obtain reproducible results. † Thus, in this manner, the WPMR analysis results are brought closer to the realistic structural conditions.

The coefficient of friction (μ) between the pedestal supports and the pool floor is indeterminate. According to Rabinowicz [6.5.1], results of 199 tests performed on austenitic stainless steel plates submerged in water show a mean value of μ to be 0.503 with standard deviation of 0.125.

† It is noted that DYNARACK has the capability to change the coefficient of friction at any pedestal at each instant of contact based on a random reading of the computer clock cycle. However, exercising this option would yield results that could not be reproduced. Therefore, the random choice of coefficients is made only once per run.

Upper and lower bounds (based on twice standard deviation) are 0.753 and 0.253, respectively. Analyses are therefore performed for coefficient of friction values of 0.2 (lower limit), 0.8 (upper limit), and for random friction values clustered about a mean of 0.5. The bounding values of μ = 0.2 and 0.8 have been found to envelope the upper limit of module response in previous rerack projects.

The bearing pads, which are inserted between the support pedestals and the pool liner, may require additional shim plates in order to span liner weld seams. These shims will be welded to the bearing pads prior to final installation in the spent fuel pool. The presence of these shims does not affect the range of friction coefficients that is used in the dynamic rack simulations. If sliding does occur, the bearing pad is expected to remain stationary as the support pedestal moves on its surface. This is because the interface between the bearing pad and the support pedestal is the only friction surface that involves two different materials. The liner plate, the bearing pads, and the shim plates are all fabricated with SA240-304 stainless steel, whereas the support pedestal is fabricated with SA564-630 stainless steel.

6.6.4 Governing Equations of Motion

Using the structural model discussed in the foregoing, equations of motion corresponding to each degree-of-freedom are obtained using Lagrange's Formulation [6.6.1]. The system kinetic energy includes contributions from solid structures and from trapped and surrounding fluid. The final system of equations obtained have the matrix form:

$$[M]\left[\frac{d^2q}{dt^2}\right] = [Q] + [G]$$

where:

[M] - total mass matrix (including structural and fluid mass contributions). The size of this matrix will be 22n x22n for a WPMR analysis (n = number of racks in the model).

q - the nodal displacement vector relative to the pool slab displacement (the term with q indicates the second derivative with respect to time, i.e., acceleration)

[G] - a vector dependent on the given ground acceleration

[Q] - a vector dependent on the spring forces (linear and nonlinear) and the coupling between degrees-of-freedom

The above column vectors have length 22n. The equations can be rewritten as follows:

$$\left[\frac{d^2q}{dt^2}\right] = [M]^{-1}[Q] + [M]^{-1}[G]$$

This equation set is mass uncoupled, displacement coupled at each instant in time. The numerical solution uses a central difference scheme built into the proprietary computer program DYNARACK [6.2.4].

No convergence problems were experienced during any of the simulations. As demonstrated during an intensive NRC review of DYNARACK in the V.C. Summer station rerack license (ca. 1983) the central difference iteration scheme used in DYNARACK ensures that the solution will be unconditionally convergent. DYNARACK has been used to perform over 2000 seismic simulations of fuel racks in more than 40 dockets over the past 20 years. Stability is achieved after a certain minimum time step (interval between solutions) is established. The time step is chosen based on previous experience with the solver and is adjusted during the initial runs if solutions are not obtained.

6.7 Structural Evaluation of Spent Fuel Rack Design

6.7.1 Kinematic and Stress Acceptance Criteria

There are two sets of criteria to be satisfied by the rack modules:

a. Kinematic Criteria

An isolated fuel rack situated in the middle of the storage cavity is most vulnerable to overturning because such a rack would be hydrodynamically uncoupled from any adjacent structures. Therefore, to assess the margin against overturning, a single rack module is evaluated. According to the O.T. Position paper (USNRC, ca 1978), the minimum required safety margins under the OBE and SSE events is 1.5 and 1.1, respectively. The maximum rotation of the rack (about its two principal axes) is obtained from a post processing of the rack time history response output. The ratio of the rotation required to produce incipient tipping in either principal plane to the actual maximum rotation in that plane from

the time history solution is the margin of safety. All ratios available for the OBE and SSE events should be greater than 1.5 and 1.1, respectively to satisfy the regulatory acceptance criteria.

b. Stress Limit Criteria

Stress limits must not be exceeded under the postulated load combinations provided herein.

6.7.2 Stress Limit Evaluations

The stress limits presented below apply to the rack structure and are derived from the ASME Code, Section III, Subsection NF [6.7.1]. Parameters and terminology are in accordance with the ASME Code. Material properties are obtained from the ASME Code Appendices [6.7.2], and are listed in Table 6.3.1.

(i) Normal and Upset Conditions (Level A or Level B)

a. Allowable stress in tension on a net section is:

$F_t = 0.6\ S_y$

Where, S_y = yield stress at temperature, and F_t is equivalent to primary membrane stress.

b. Allowable stress in shear on a net section is:

$F_v = .4\ S_y$

c. Allowable stress in compression on a net section

$$F_a = S_y \left(.47 - \frac{k\lambda}{444\,r} \right)$$

$k\lambda/r$ for the main rack body is based on the full height and cross section of the honeycomb region and does not exceed 120 for all sections.

λ = unsupported length of component

k = length coefficient which gives influence of boundary conditions. The following values are appropriate for the described end conditions:

= 1 (simple support both ends)

= 2 (cantilever beam)

= ½ (clamped at both ends)

r = radius of gyration of component

d. Maximum allowable bending stress at the outermost fiber of a net section, due to flexure about one plane of symmetry is:

$F_b = 0.60\ S_y$ (equivalent to primary bending)

e. Combined bending and compression on a net section satisfies:

$$\frac{f_a}{F_a} + \frac{C_{mx}\ f_{bx}}{D_x\ F_{bx}} + \frac{C_{my}\ f_{by}}{D_y\ F_{by}} < 1$$

where:

f_a = Direct compressive stress in the section

f_{bx} = Maximum bending stress along x-axis

f_{by} = Maximum bending stress along y-axis

C_{mx} = 0.85

C_{my} = 0.85

D_x = $1 - (f_a/F'_{ex})$

D_y = $1 - (f_a/F'_{ey})$

$F'_{ex,ey}$ = $(\pi^2 E)/(2.15\ (kl/r)^2_{x,y})$

E = Young's Modulus

and subscripts x,y reflect the particular bending plane.

f. Combined flexure and compression (or tension) on a net section:

$$\frac{f_a}{0.6\,S_y} + \frac{f_{bx}}{F_{bx}} + \frac{f_{by}}{F_{by}} < 1.0$$

The above requirements are to be met for both direct tension or compression.

g. Welds

Allowable maximum shear stress on the net section of a weld is given by:

$$F_w = 0.3\ S_u$$

where S_u is the weld material ultimate strength at temperature. For fillet weld legs in contact with base metal, the shear stress on the gross section is limited to $0.4S_y$, where S_y is the base material yield strength at temperature.

(ii) Level D Service Limits

Section F-1334 (ASME Section III, Appendix F) [6.7.2], states that the limits for the Level D condition are the minimum of 1.2 (S_y/F_t) or 0.7 (S_u/F_t) times the corresponding limits for the Level A condition. S_u is ultimate tensile stress at the specified rack design temperature. Examination of material properties for 304L stainless steel demonstrates that 1.2 times the yield strength is less than the 0.7 times the ultimate strength.

Exceptions to the above general multiplier are the following:

a) Stresses in shear shall not exceed the lesser of $0.72S_y$ or $0.42S_u$. In the case of the austenitic stainless steel material used here, $0.72S_y$ governs.

b) Axial Compression Loads shall be limited to 2/3 of the calculated buckling load.

c) Combined Axial Compression and Bending - The equations for Level A conditions shall apply except that:

F_a = 0.667 x Buckling Load/ Gross Section Area,

and the terms F'_{ex} and F'_{ey} may be increased by the factor 1.65.

d) For welds, the Level D allowable maximum weld stress is not specified in Appendix F of the ASME Code. An appropriate limit for weld throat stress is conservatively set here as:

$F_w = (0.3\ S_u)$ x factor

where:

factor = (Level D shear stress limit)/(Level A shear stress limit)

6.7.3 Dimensionless Stress Factors

For convenience, the stress results are presented in dimensionless form. Dimensionless stress factors are defined as the ratio of the actual developed stress to the specified limiting value. The limiting value of each stress factor is 1.0, based on the allowable strengths for each level, for Levels A, B, and D (where $1.2S_y < .7S_u$). Stress factors reported are:

R_1 = Ratio of direct tensile or compressive stress on a net section to its allowable value (note pedestals only resist compression)

R_2 = Ratio of gross shear on a net section in the x-direction to its allowable value

R_3 = Ratio of maximum x-axis bending stress to its allowable value for the section

R_4 = Ratio of maximum y-axis bending stress to its allowable value for the section

R_5 = Combined flexure and compressive factor (as defined in the foregoing)

R_6 = Combined flexure and tension (or compression) factor (as defined in the foregoing)

R_7 = Ratio of gross shear on a net section in the y-direction to its allowable value

6.7.4 Loads and Loading Combinations for Spent Fuel Racks

The applicable loads and their combinations which must be considered in the seismic analysis of rack modules is excerpted from Refs. [6.1.2] and [6.7.3]. The load combinations considered are identified below:

Loading Combination	Service Level
$D + L$ $D + L + T_o$ $D + L + T_o + E$	Level A
$D + L + T_a + E$ $D + L + T_o + P_f$	Level B
$D + L + T_a + E'$ $D + L + T_o + F_d$	Level D The functional capability of the fuel racks must be demonstrated.

where:

D = Dead weight-induced loads (including fuel assembly weight)

L = Live Load (not applicable for the fuel rack, since there are no moving objects in the rack load path)

P_f = Upward force on the racks caused by postulated stuck fuel assembly

F_d = Impact force from accidental drop of the heaviest load from the maximum possible height.

E = Operating Basis Earthquake (OBE)

E' = Safe Shutdown Earthquake (SSE)

T_o = Differential temperature induced loads (normal operating or shutdown condition based on the most critical transient or steady state condition)

T_a = Differential temperature induced loads (the highest temperature associated with the postulated abnormal design conditions)

T_a and T_o produce local thermal stresses. The worst thermal stress field in a fuel rack is obtained when an isolated storage location has a fuel assembly generating heat at maximum postulated rate and surrounding storage locations contain no fuel. Heated water makes unobstructed contact with the inside of the storage walls, thereby producing maximum possible temperature difference between adjacent cells. Secondary stresses produced are limited to the body of the rack; that is, support pedestals do not experience secondary (thermal) stresses.

6.8 Parametric Simulations

Consideration of the parameters described above results in a number of scenarios for both the WPMR and the Single Rack analyses. The single rack analysis considers only one rack in the analysis model whereas the WPMR analysis considers all racks in the model. Since the proposed pool layout and rack modules for both plants are exactly alike, the set of WPMR and Single Rack models developed for one plant is equally valid for the other plant. The pool layout is shown in Figure 2.1. The rack numbering scheme used in the dynarack model for WPMR simulation is introduced in Figure 6.8.1 along with the gap spring numbering scheme.

The Single Rack analysis considers the heaviest rack module and the rack module with highest aspect ratio (i.e. the ratio of length to width of a rack). Rack K (one of the heaviest racks) and Rack J (featuring the highest aspect ratio) are selected for single rack analysis. The single rack model with the heaviest rack is most likely to produce the largest pedestal loads while the model with the highest aspect ratio rack is highly susceptible to large displacements using the Single Rack method. In addition to these Single Rack simulations, a Single Rack run that exhibits the greatest displacement is re-run solely for the purpose of checking the potential for overturning. The table below presents a complete listing of the simulations discussed herein.

LIST OF RACK SIMULATIONS

Run	Model	Load Case	COF	Event
1	WPMR	Full Pool	0.2	SSE
2	WPMR	Full Pool	0.8	SSE
3	WPMR	Full Pool	Random	SSE
4	WPMR	Full Pool	0.2	OBE
5	WPMR	Full Pool	0.8	OBE
6	WPMR	Full Pool	Random	OBE
7	Single Rack (J)	Full Rack	0.8	SSE
8	Single Rack (J)	Full Rack	0.2	SSE
9	Single Rack (J)	Half-Full Rack (symmetric about short axis)	0.8	SSE
10	Single Rack (J)	Half-Full Rack (symmetric about short axis)	0.2	SSE
11	Single Rack (J)	Nearly Empty	0.8	SSE

LIST OF RACK SIMULATIONS				
Run	**Model**	**Load Case**	**COF**	**Event**
12	Single Rack (J)	Nearly Empty	0.2	SSE
13	Single Rack (K)	Full Rack	0.8	SSE
14	Single Rack (K)	Full Rack	0.2	SSE
15	Single Rack (K)	Half-Full Rack (symmetric about short axis)	0.8	SSE
16	Single Rack (K)	Half-Full Rack (symmetric about short axis)	0.2	SSE
17	Single Rack (K)	Nearly Empty	0.8	SSE
18	Single Rack (K)	Nearly Empty	0.2	SSE
19	Single Rack (J)	Full Rack	0.8	OBE
20	Single Rack (J)	Full Rack	0.2	OBE
21	Single Rack (J)	Half-Full Rack (symmetric about short axis)	0.8	OBE
22	Single Rack (J)	Half-Full Rack (symmetric about short axis)	0.2	OBE
23	Single Rack (J)	Nearly Empty	0.8	OBE
24	Single Rack (J)	Nearly Empty	0.2	OBE
25	Single Rack (K)	Full Rack	0.8	OBE
26	Single Rack (K)	Full Rack	0.2	OBE
27	Single Rack (K)	Half-Full Rack (symmetric about short axis)	0.8	OBE
28	Single Rack (K)	Half-Full Rack (symmetric about short axis)	0.2	OBE
29	Single Rack (K)	Nearly Empty	0.8	OBE
30	Single Rack (K)	Nearly Empty	0.2	OBE
31	Single Rack Overturning Check (K)	Full Rack	0.8	SSE

where:

Random = Gaussian distribution with a mean coefficient of friction (COF) of 0.5 and a standard deviation equal to 0.15.

Note that Run No. 31 is a re-run of Run No. 13 except that the rack module in this run is simulated as an isolated rack in the pool as described earlier in subsection 6.7.1.

6.9 Time History Simulation Results

The results from the DYNARACK runs may be seen in the raw data output files. However, due to the huge quantity of output data, a post-processor is used to scan for worst case conditions and develop the stress factors. Further reduction in this bulk of information is provided in this section by extracting the worst case values from the parameters of interest; namely displacements, support pedestal forces, impact loads, and stress factors. This section also summarizes other analyses performed to develop and evaluate structural member stresses which are not determined by the post processor. For each table, the Pool Condition/COF column refers to whether the pool is full, half full or nearly empty (a few cells loaded). COF is the interface coefficient of friction discussed in subsection 6.2.1. The "Rack" column denotes racks by number (applicable to the DYNARACK model) and by letter (applicable to the pool layout drawing).

6.9.1 Rack Displacements

A tabulated summary of the maximum displacement for each simulation is provided below. It is noted that all of the maximum displacements occurred at the tops of the storage racks, as expected, from swaying, bending and tipping. The location/direction terms are defined as follows:

uxt, uyt = displacement of top corner of rack, relative to the slab, in the North-South and East-West directions, respectively, in the Braidwood pool. The maximum displacements for every simulation, including the single rack tipover run, occurred at the top of the racks shown in the last table column.

RACK DISPLACEMENT RESULTS						
Run	**Model**	**Pool Condition/ COF**	**Event**	**Max. Disp. (in)**	**Direction**	**Rack**
1	WPMR	Full/0.2	SSE	0.688	uyt	14(P)
2	WPMR	Full/0.8	SSE	0.865	uxt	12(M)
3	WPMR	Full/Rand.	SSE	0.823	uxt	12(M)
4	WPMR	Full/0.2	OBE	0.468	uyt	12(M)
5	WPMR	Full/0.8	OBE	0.467	uyt	12(M)
6	WPMR	Full/Rand.	OBE	0.467	uyt	12(M)
7	Single Rack	Full/0.8	SSE	0.234	uyt	9(J)
8	Single Rack	Full/0.2	SSE	0.207	uyt	9(J)
9	Single Rack	Half/0.8	SSE	0.124	uyt	9(J)
10	Single Rack	Half/0.2	SSE	0.116	uyt	9(J)
11	Single Rack	Empty/0.8	SSE	0.0256	uyt	9(J)
12	Single Rack	Empty/0.2	SSE	0.0232	uyt	9(J)
13	Single Rack	Full/0.8	SSE	0.162	uxt	10(K)
14	Single Rack	Full/0.2	SSE	0.143	uxt	10(K)
15	Single Rack	Half/0.8	SSE	0.0766	uxt	10(K)
16	Single Rack	Half/0.2	SSE	0.0682	uyt	10(K)
17	Single Rack	Empty/0.8	SSE	0.0262	uyt	10(K)
18	Single Rack	Empty/0.2	SSE	0.0265	uyt	10(K)
19	Single Rack	Full/0.8	OBE	0.09	uxt	9(J)
20	Single Rack	Full/0.2	OBE	0.0897	uxt	9(J)
21	Single Rack	Half/0.8	OBE	0.0665	uxt	9(J)
22	Single Rack	Half/0.2	OBE	0.0634	uxt	9(J)
23	Single Rack	Empty/0.8	OBE	0.0118	uxt	9(J)
24	Single Rack	Empty/0.2	OBE	0.0121	uxt	9(J)
25	Single Rack	Full/0.8	OBE	0.0915	uyt	10(K)
26	Single Rack	Full/0.2	OBE	0.072	uyt	10(K)
27	Single Rack	Half/0.8	OBE	0.058	uyt	10(K)

RACK DISPLACEMENT RESULTS						
Run	**Model**	**Pool Condition/ COF**	**Event**	**Max. Disp. (in)**	**Direction**	**Rack**
28	Single Rack	Half/0.2	OBE	0.050	uyt	10(K)
29	Single Rack	Empty/0.8	OBE	0.0148	uyt	10(K)
30	Single Rack	Empty/0.2	OBE	0.0145	uyt	10(K)
31	Single Rack	Single Rack Overturning Check	SSE	1.500	uyt	10(K)

The table shows that the maximum rack displacement is 1.50 inches (Run 31). With this given value, an evaluation of rack overturning is performed. The factor of safety obtained from this evaluation is 61, which is much higher than the prescribed limit of 1.5 for OBE conditions. This indicates that tipover is not a concern. Table 6.9.1 shows the maximum calculated and maximum allowed rotation of the rack.

The maximum rack displacements at the baseplate elevation are 0.5975 inches (Run No. 1) and 0.2358 inches (Run No. 4) for the SSE event and the OBE event, respectively.

The displacement shape of each rack, from the baseplate elevation to the top of the rack, is nearly linear. This indicates that the primary displacement mode of the fuel racks is rigid body motion (i.e., sliding and tilting). In other words, the elastic deformation of the cell structure due to bending is negligible compared to the rigid body displacements.

6.9.2 Pedestal Vertical Load

Pedestal number 1 for each rack is located in the northeast and the southwest corner of racks of the Braidwood and Byron station, respectively. Numbering increases counterclockwise around the periphery of each rack. The following bounding vertical pedestal forces are obtained for each run:

MAXIMUM VERTICAL LOADS					
Run	**Model**	**Pool Condition/ COF**	**Event**	**Max. Vertical Load (lb)**	**Rack**
1	WPMR	Full/0.2	SSE	198000	18(T)
2	WPMR	Full/0.8	SSE	229000	18(T)
3	WPMR	Full/Rand.	SSE	238000	2(B)
4	WPMR	Full/0.2	OBE	131000	23(Y)
5	WPMR	Full/0.8	OBE	144000	11(L)
6	WPMR	Full/Rand.	OBE	144000	11(L)
7	Single Rack	Full/0.8	SSE	169000	9(J)
8	Single Rack	Full/0.2	SSE	131000	9(J)
9	Single Rack	Half/0.8	SSE	78200	9(J)
10	Single Rack	Half/0.2	SSE	68700	9(J)
11	Single Rack	Empty/0.8	SSE	15000	9(J)
12	Single Rack	Empty/0.2	SSE	13900	9(J)
13	Single Rack	Full/0.8	SSE	109000	10(K)
14	Single Rack	Full/0.2	SSE	101000	10(K)
15	Single Rack	Half/0.8	SSE	52900	10(K)
16	Single Rack	Half/0.2	SSE	56500	10(K)
17	Single Rack	Empty/0.8	SSE	20600	10(K)
18	Single Rack	Empty/0.2	SSE	19600	10(K)
19	Single Rack	Full/0.8	OBE	92300	9(J)
20	Single Rack	Full/0.2	OBE	92500	9(J)
21	Single Rack	Half/0.8	OBE	51400	9(J)
22	Single Rack	Half/0.2	OBE	51300	9(J)
23	Single Rack	Empty/0.8	OBE	10800	9(J)
24	Single Rack	Empty/0.2	OBE	10900	9(J)
25	Single Rack	Full/0.8	OBE	81400	10(K)
26	Single Rack	Full/0.2	OBE	79700	10(K)
27	Single Rack	Half/0.8	OBE	42800	10(K)

MAXIMUM VERTICAL LOADS					
Run	**Model**	**Pool Condition/ COF**	**Event**	**Max. Vertical Load (lb)**	**Rack**
28	Single Rack	Half/0.2	OBE	42800	10(K)
29	Single Rack	Empty/0.8	OBE	14500	10(K)
30	Single Rack	Empty/0.2	OBE	14300	10(K)

The highest maximum vertical pedestal loads from all simulations for the SSE and OBE conditions are 238,000 lbs and 144,000 lbs, respectively. The effect of these loads is evaluated in bearing pad and rack fatigue analyses.

6.9.3 Pedestal Friction Forces

The maximum (x or y direction) shear load bounding all pedestals in the simulation are reported below and are obtained by compilation of the complete tabular data produced by time history solution of whole pool multirack and single rack simulations.

MAXIMUM HORIZONTAL LOADS					
Run	**Model**	**Pool Condition/ COF**	**Event**	**Max. Shear Load (lb)**	**Rack**
1	WPMR	Full/0.2	SSE	33200	20(V)
2	WPMR	Full/0.8	SSE	101000	11(L)
3	WPMR	Full/Rand.	SSE	83300	3(C)
4	WPMR	Full/0.2	OBE	24200	16(R)
5	WPMR	Full/0.8	OBE	50100	3(C)
6	WPMR	Full/Rand.	OBE	48500	4(D)
7	Single Rack	Full/0.8	SSE	55200	9(J)
8	Single Rack	Full/0.2	SSE	24600	9(J)
9	Single Rack	Half/0.8	SSE	33800	9(J)
10	Single Rack	Half/0.2	SSE	13200	9(J)
11	Single Rack	Empty/0.8	SSE	4990	9(J)

MAXIMUM HORIZONTAL LOADS					
Run	**Model**	**Pool Condition/ COF**	**Event**	**Max. Shear Load (lb)**	**Rack**
12	Single Rack	Empty/0.2	SSE	2740	9(J)
13	Single Rack	Full/0.8	SSE	50000	10(K)
14	Single Rack	Full/0.2	SSE	20000	10(K)
15	Single Rack	Half/0.8	SSE	19200	10(K)
16	Single Rack	Half/0.2	SSE	9720	10(K)
17	Single Rack	Empty/0.8	SSE	6270	10(K)
18	Single Rack	Empty/0.2	SSE	3600	10(K)
19	Single Rack	Full/0.8	OBE	10000	9(J)
20	Single Rack	Full/0.2	OBE	16000	9(J)
21	Single Rack	Half/0.8	OBE	7540	9(J)
22	Single Rack	Half/0.2	OBE	10100	9(J)
23	Single Rack	Empty/0.8	OBE	1380	9(J)
24	Single Rack	Empty/0.2	OBE	1940	9(J)
25	Single Rack	Full/0.8	OBE	8660	10(K)
26	Single Rack	Full/0.2	OBE	11800	10(K)
27	Single Rack	Half/0.8	OBE	14600	10(K)
28	Single Rack	Half/0.2	OBE	8170	10(K)
29	Single Rack	Empty/0.8	OBE	2130	10(K)
30	Single Rack	Empty/0.2	OBE	2390	10(K)

The largest horizontal pedestal load of 101,000 lbs occurs in run 2. The effect of this load is evaluated in the liner fatigue analysis.

6.9.4 Rack Impact Loads

A freestanding rack, by definition, is a structure subject to potential impacts during a seismic event. Impacts arise from rattling of the fuel assemblies in the storage rack locations and, in some instances, from localized impacts between the racks, or between a peripheral rack and the pool wall.

Results of simulations predict no impact (in the rack cellular region) between racks, or with walls under any simulation. The time history solution does indicate the occurrence of localized impacts at rack baseplate location. The maximum local rack-bottom impact force from each set are reported as follows:

Run	Impact Force, lbf	Analysis
2	80,070	WPMR
8	13,980	SINGLE RACK

The rack baseplates, which are manufactured from a continuous steel plate, which is 0.75 inch thick, can sustain impacts at the baseplate level that are greater than the forces listed above. The compressive stress in the baseplate due to the maximum impact load of 80,070 lbs is 8,897 psi, which is less than the yield stress of the baseplate material (21,300 psi). Therefore, the calculated rack-to-rack impact loads at the baseplate are acceptable.

6.9.4.1 Fuel to Cell Wall Impact Loads

As discussed in subsection 6.5.1 the fuel assemblies are modelled using five lumped masses. Each of these masses interacts with the rack via four nonlinear compression only spring elements. These elements are termed nonlinear, since they have the capability of being inactive (non-load bearing) until the fuel assembly mass comes in contact with the cell wall. The loads developed by these elements are conservative, since the actual assembly to cell wall impacts will be experienced at the assembly spacer grids. Since the number of spacer grids are greater than the number of lumped masses used in the model, the impact loadings will actually occur at more locations, resulting in lower loads at each point of contact.

The DYNARACK program produces a complete time history of the loadings within these non-linear compression only gap/spring elements and archives the results for later review or post-processing. Post-processors enable scanning of the large number of time steps for instants where loads are actually present and allows for easy retrieval of the bounding values.

Fuel assembly integrity is assured by comparing the calculated impact load against manufacturers test data for assembly grid side loadings. Additionally, it should be noted that the impact loads experienced by the fuel assemblies from postulated seismic event during storage in

the racks is expected to be exceeded by the loadings experienced during service within the reactor under similar events as previously analyzed and accepted during original plant licensing.

The cell wall integrity is determined by comparison of the calculated load with an allowable impact load developed using plastic analysis of the local cell wall impact zone.

The fluid coupling between the fuel assembly and the cell wall is treated by inertial coupling in the system kinetic energy. The methodology is taken from classical mechanics as described by Fritz in, "The Effects of Liquids on the Dynamic Motions of Immersed Solids" [6.5.3]and by Singh and Soler in "Dynamic Coupling in a Closely Spaced Two-Body System Vibrating in Liquid Medium: The Case of Fuel Racks" [6.5.2].

A review of all simulations performed allows determination of the maximum instantaneous impact load between fuel assembly and fuel cell wall at any modeled impact site. The maximum fuel to cell wall impact load values are reported in the following table.

FUEL-TO-CELL WALL IMPACT					
Run	**Model**	**Pool Condition/ COF**	**Event**	**Impact Load (lb)**	**Rack**
1	WPMR	Full/0.2	SSE	822	4(D)
2	WPMR	Full/0.8	SSE	830	4(D)
3	WPMR	Full/Rand.	SSE	828	4(D)
4	WPMR	Full/0.2	OBE	428	10(K)
5	WPMR	Full/0.8	OBE	45[illegible]	4(D)
6	WPMR	Full/Rand.	OBE	[illegible]8	4(D)
7	Single Rack	Full/0.8	SSE	55[illegible]	9(J)
8	Single Rack	Full/0.2	SSE	570	9(J)
9	Single Rack	Half/0.8	SSE	529	9(J)
10	Single Rack	Half/0.2	SSE	514	9(J)
11	Single Rack	Empty/0.8	SSE	48[illegible]	9(J)
12	Single Rack	Empty/0.2	SSE	565	9(J)
13	Single Rack	Full/0.8	SSE	829	10(K)

FUEL-TO-CELL WALL IMPACT					
Run	**Model**	**Pool Condition/ COF**	**Event**	**Impact Load (lb)**	**Rack**
14	Single Rack	Full/0.2	SSE	822	10(K)
15	Single Rack	Half/0.8	SSE	780	10(K)
16	Single Rack	Half/0.2	SSE	559	10(K)
17	Single Rack	Empty/0.8	SSE	808	10(K)
18	Single Rack	Empty/0.2	SSE	448	10(K)
19	Single Rack	Full/0.8	OBE	292	9(J)
20	Single Rack	Full/0.2	OBE	291	9(J)
21	Single Rack	Half/0.8	OBE	329	9(J)
22	Single Rack	Half/0.2	OBE	341	9(J)
23	Single Rack	Empty/0.8	OBE	1148	9(J)
24	Single Rack	Empty/0.2	OBE	1113	9(J)
25	Single Rack	Full/0.8	OBE	387	10(K)
26	Single Rack	Full/0.2	OBE	389	10(K)
27	Single Rack	Half/0.8	OBE	893	10(K)
28	Single Rack	Half/0.2	OBE	893	10(K)
29	Single Rack	Empty/0.8	OBE	1118	10(K)
30	Single Rack	Empty/0.2	OBE	1120	10(K)

The maximum fuel-to-cell wall impact load is recorded to be 1,148 lbs during run no. 23. The structural integrity of the cell wall under the impact of this load is evaluated. The discussion of this evaluation is provided in section 6.10.3 of this report.

The permissible lateral load on an irradiated spent fuel assembly has been studied by the Lawrence Livermore National Laboratory. The LLNL report [6.10.1] states that "…for the most vulnerable fuel assembly, axial buckling varies from 82g's at initial storage to 95g's after 20 years' storage. In a side drop, no yielding is expected below 63g's at initial storage to 74g's after 20 years' [dry] storage". The most significant load on the fuel assembly arises from rattling during the seismic event. For the five lumped mass model, the limiting lateral load, therefore, is equal to F_e, where

$$F_e = (w \times a)/5$$

where:

w = weight of one fuel assembly (upper bound value = 1600 lbs)

a = permissible lateral acceleration in g's (a = 63)

Therefore, F_e = 20,160 lbs.

The maximum fuel-to-cell wall impact force from the array of parametric runs listed in the above table is 1,148 lbs. Therefore, the nominal factor of safety against Spent Nuclear Fuel (SNF) failure is computed to be 17.

6.9.5 Rack Vertical Displacement

A tabulated summary of the maximum vertical displacement for each simulation is provided below. Note that these displacements represent the rack lift-off during the seismic event, as a result of rocking, sliding, swaying, bending, and tipping behavior of the rack module.

RACK VERTICAL DISPLACEMENT RESULTS						
Run	**Model**	**Pool Condition/ COF**	**Event**	**Max. Vertical Disp. (in)**	**direction**	**Rack**
1	WPMR	Full/0.2	SSE	0.0998	upward	23/Y
2	WPMR	Full/0.8	SSE	[illegible]1334	upward	2/B
3	WPMR	Full/Rand.	SSE	0.1301	upward	11/L
4	WPMR	Full/0.2	OBE	0.0754	upward	21/W
5	WPMR	Full/0.8	OBE	0.0766	upward	21/W
6	WPMR	Full/Rand.	OBE	0.0761	upward	21/W
7	Single Rack	Full/0.8	SSE	0.087	upward	9(J)
8	Single Rack	Full/0.2	SSE	0.087	upward	9(J)
9	Single Rack	Half/0.8	SSE	0.043	upward	9(J)
10	Single Rack	Half/0.2	SSE	0.0426	upward	9(J)

RACK VERTICAL DISPLACEMENT RESULTS						
Run	**Model**	**Pool Condition/ COF**	**Event**	**Max. Vertical Disp. (in)**	**direction**	**Rack**
11	Single Rack	Empty/0.8	SSE	0.0084	upward	9(J)
12	Single Rack	Empty/0.2	SSE	0.0084	upward	9(J)
13	Single Rack	Full/0.8	SSE	0.0443	upward	10(K)
14	Single Rack	Full/0.2	SSE	0.0431	upward	10(K)
15	Single Rack	Half/0.8	SSE	0.020	upward	10(K)
16	Single Rack	Half/0.2	SSE	0.0219	upward	10(K)
17	Single Rack	Empty/0.8	SSE	0.0070	upward	10(K)
18	Single Rack	Empty/0.2	SSE	0.0069	upward	10(K)
19	Single Rack	Full/0.8	OBE	0.0675	upward	9(J)
20	Single Rack	Full/0.2	OBE	0.0675	upward	9(J)
21	Single Rack	Half/0.8	OBE	0.0343	upward	9(J)
22	Single Rack	Half/0.2	OBE	0.0343	upward	9(J)
23	Single Rack	Empty/0.8	OBE	0.0069	upward	9(J)
24	Single Rack	Empty/0.2	OBE	0.0069	upward	9(J)
25	Single Rack	Full/0.8	OBE	0.0344	upward	10(K)
26	Single Rack	Full/0.2	OBE	0.0344	upward	10(K)
27	Single Rack	Half/0.8	OBE	0.0176	upward	10(K)
28	Single Rack	Half/0.2	OBE	0.0176	upward	10(K)
29	Single Rack	Empty/0.8	OBE	0.0058	upward	10(K)
30	Single Rack	Empty/0.2	OBE	0.0058	upward	10(K)
31	Single Rack	Single Rack Overturning Check	SSE	0.3199	upward	10(K)

The maximum vertical displacement is 0.3199 inches which occurs in run No. 31.

6.10 Rack Structural Evaluation

6.10.1 Rack Stress Factors

With time history results available for pedestal normal and lateral interface forces, the maximum values for the previously defined stress factors can be determined for every pedestal in the array of racks. With this information available, the structural integrity of the pedestal can be assessed and reported. The net section maximum (in time) bending moments and shear forces can also be determined at the bottom casting-rack cellular structure interface for each spent fuel rack in the pool. With this information in hand, the maximum stress in the most stressed rack cell (box) can be evaluated.

An evaluation of the stress factors for all of the simulations performed leads to the conclusion that all stress factors are less than the mandated limit of 1.0 for the load cases examined. From all of the simulations, the bounding stress factors for each run, in either the cellular or the pedestal region, are summarized below :

MAXIMUM STRESS FACTORS					
Run	**Model**	**Pool Condition/ COF**	**Event**	**Stress Factor**	**Rack/ Factor Type**
1	WPMR	Full/0.2	SSE	0.252	18(T)/R5
2	WPMR	Full/0.8	SSE	0.443	3(C)/R6
3	WPMR	Full/Rand.	SSE	0.407	11(L)/R6
4	WPMR	Full/0.2	OBE	0.428	12(M)/R6
5	WPMR	Full/0.8	OBE	0.494	12(M)/R6
6	WPMR	Full/Rand.	OBE	0.459	12(M)/R6
7	Single Rack	Full/0.8	SSE	0.302	9(J)/R6
8	Single Rack	Full/0.2	SSE	0.173	9(J)/R6
9	Single Rack	Half/0.8	SSE	0.140	9(J)/R6
10	Single Rack	Half/0.2	SSE	0.091	9(J)/R5
11	Single Rack	Empty/0.8	SSE	0.025	9(J)/R6
12	Single Rack	Empty/0.2	SSE	0.018	9(J)/R5

MAXIMUM STRESS FACTORS					
Run	**Model**	**Pool Condition/ COF**	**Event**	**Stress Factor**	**Rack/ Factor Type**
13	Single Rack	Full/0.8	SSE	0.248	10(K)/R6
14	Single Rack	Full/0.2	SSE	0.125	10(K)/R5
15	Single Rack	Half/0.8	SSE	0.087	10(K)/R6
16	Single Rack	Half/0.2	SSE	0.067	10(K)/R5,R6
17	Single Rack	Empty/0.8	SSE	0.028	10(K)/R5
18	Single Rack	Empty/0.2	SSE	0.023	10(K)/R5
19	Single Rack	Full/0.8	OBE	0.228	9(J)/R5
20	Single Rack	Full/0.2	OBE	0.229	9(J)/R5
21	Single Rack	Half/0.8	OBE	0.131	9(J)/R5
22	Single Rack	Half/0.2	OBE	0.130	9(J)/R5
23	Single Rack	Empty/0.8	OBE	0.028	9(J)/R5
24	Single Rack	Empty/0.2	OBE	0.029	9(J)/R5
25	Single Rack	Full/0.8	OBE	0.170	10(K)/R5
26	Single Rack	Full/0.2	OBE	0.169	10(K)/R5
27	Single Rack	Half/0.8	OBE	0.137	10(K)/R6
28	Single Rack	Half/0.2	OBE	0.103	10(K)/R5
29	Single Rack	Empty/0.8	OBE	0.031	10(K)/R5,R6
30	Single Rack	Empty/0.2	OBE	0.032	10(K)/R5

The maximum stress factor scanned from above table is 0.443 for SSE and 0.494 for OBE, which is below the prescribed Code limit of 1.0. Therefore, the stress allowables are indeed satisfied for the load levels considered for every limiting location in every rack in the array.

6.10.2 Pedestal Thread Shear Stress

The complete post-processor results give thread stresses under faulted conditions for every pedestal for every rack in the pool. The average shear stress in the engagement region is given below for the limiting pedestal in each simulation.

THREAD SHEAR STRESS					
Run	**Model**	**Pool Condition/ COF**	**Event**	**Stress (psi)**	**Rack Number**
1	WPMR	Full/0.2	SSE	8404	18(T)
2	WPMR	Full/0.8	SSE	9719	18(T)
3	WPMR	Full/Rand.	SSE	10102	2(B)
4	WPMR	Full/0.2	OBE	5560	23(Y
5	WPMR	Full/0.8	OBE	6112	11(L)
6	WPMR	Full/Rand.	OBE	6112	11(L)
7	Single Rack	Full/0.8	SSE	7173	9(J)
8	Single Rack	Full/0.2	SSE	5560	9(J)
9	Single Rack	Half/0.8	SSE	3319	9(J)
10	Single Rack	Half/0.2	SSE	2916	9(J)
11	Single Rack	Empty/0.8	SSE	637	9(J)
12	Single Rack	Empty/0.2	SSE	590	9(J)
13	Single Rack	Full/0.8	SSE	4626	10(K)
14	Single Rack	Full/0.2	SSE	4287	10(K)
15	Single Rack	Half/0.8	SSE	2245	10(K)
16	Single Rack	Half/0.2	SSE	2398	10(K)
17	Single Rack	Empty/0.8	SSE	874	10(K)
18	Single Rack	Empty/0.2	SSE	832	10(K)
19	Single Rack	Full/0.8	OBE	3918	9(J)
20	Single Rack	Full/0.2	OBE	3926	9(J)
21	Single Rack	Half/0.8	OBE	2181	9(J)
22	Single Rack	Half/0.2	OBE	2177	9(J)
23	Single Rack	Empty/0.8	OBE	458	9(J)
24	Single Rack	Empty/0.2	OBE	462	9(J)
25	Single Rack	Full/0.8	OBE	3455	10(K)
26	Single Rack	Full/0.2	OBE	3383	10(K)
27	Single Rack	Half/0.8	OBE	1817	10(K)

THREAD SHEAR STRESS					
Run	**Model**	**Pool Condition/ COF**	**Event**	**Stress (psi)**	**Rack Number**
28	Single Rack	Half/0.2	OBE	1817	10(K)
29	Single Rack	Empty/0.8	OBE	615	10(K)
30	Single Rack	Empty/0.2	OBE	607	10(K)

The ultimate strength of the internally threaded part of the pedestal is 66,200 psi. The yield stress for this material is 21,300 psi. The allowable shear stress for Level B (OBE) conditions is 0.4 times the yield stress which gives 8,520 psi and the allowable shear stress for level D is 0.72 times the yield stress which gives 15,336 psi. The maximum calculated shear stress value for the SSE is 10,102 psi and 6112 psi for the OBE which are less than their respective allowables. Therefore, thread shear stresses are acceptable under all conditions.

6.10.3 Local Stresses Due to Impacts

Impact loads at the pedestal base (discussed in subsection 6.9.2) produce stresses in the pedestal for which explicit stress limits are prescribed in the Code. However, impact loads on the cellular region of the racks, as discussed in subsection 6.9.4.1 above, produce stresses which attenuate rapidly away from the loaded region. This behavior is characteristic of secondary stresses.

Even though limits on secondary stresses are not prescribed in the Code for Class 3 NF structures, evaluations must be made to ensure that the localized impacts do not lead to plastic deformations in the storage cells which affect the subcriticality of the stored fuel array.

Local cell wall integrity is conservatively estimated from peak impact loads. Plastic analysis is used to obtain the limiting impact load which would lead to gross permanent deformation. Table 6.9.1 indicates that the limiting impact load (3,698 lbf, including a safety factor of 2.0) is much greater than the highest calculated impact load value (1,148 lbf, see subsection 6.9.4.1) obtained from any of the rack analyses. Therefore, fuel impacts do not represent a concern with respect to fuel rack cell deformation.

6.10.4 Assessment of Rack Fatigue Margin

Deeply submerged high density spent fuel storage racks arrayed in close proximity to each other in a free-standing configuration behave primarily as a nonlinear cantilevered structure when subjected to 3-D seismic excitations. In addition to the pulsations in the vertical load at each pedestal, lateral friction forces at the pedestal/bearing pad-liner interface, which help prevent or mitigate lateral sliding of the rack, also exert a time-varying moment in the baseplate region of the rack. The friction-induced lateral forces act simultaneously in x and y directions with the requirement that their vectorial sum does not exceed μN where μ is the limiting interface coefficient of friction and N is the concomitant vertical thrust on the liner (at the *given* time instant). As the vertical thrust at a pedestal location changes, so does the maximum friction force, F, that the interface can exert. In other words, the lateral force at the pedestal/liner interface, F, is given by

$$F \leq \mu N(\tau)$$

where N (vertical thrust) is the time-varying function of τ. F does not always equal μN; rather, μ N is the maximum value it can attain at any time. The actual value, of course, is determined by the dynamic equilibrium of the rack structure. In summary, the horizontal friction force at the pedestal/liner interface is a function of time. Its magnitude and direction of action varies during the earthquake event.

The time-varying lateral (horizontal) and vertical forces on the extremities of the support pedestals produce stresses at the root of the pedestals in the manner of an end-loaded cantilever. The stress field in the cellular region of the rack is quite complex, with its maximum values located in the region closest to the pedestal. The maximum magnitude of the stresses depends on the severity of the pedestal end loads and on the geometry of the pedestal/rack baseplate region.

Alternating stresses in metals produce metal fatigue if the amplitude of the stress cycles is sufficiently large. In high density racks designed for sites with moderate to high postulated seismic action, the stress intensity amplitudes frequently reach values above the material endurance limit, leading to expenditure of the fatigue "usage" reserve in the material.

Because the locations of maximum stress (viz., the pedestal/rack baseplate junction) and the close placement of racks, a post-earthquake inspection of the high stressed regions in the racks is

not feasible. Therefore, the racks must be engineered to withstand multiple earthquakes without reliance on nondestructive inspections for post-earthquake integrity assessment. The fatigue life evaluation of racks is an integral aspect of a sound design.

The time-history method of analysis employed in this report provides the means to obtain a complete cycle history of the stress intensities in the highly stressed regions of the rack. Having determined the amplitude of the stress intensity cycles and their number, the cumulative damage factor, U, can be determined using the classical Miner's rule

$$U = \Sigma \frac{n_i}{N_i}$$

where n_i is the number of stress intensity cycles of amplitude σ_i, and N_i is the permissible number of cycles corresponding to σ_i from the ASME fatigue curve for the material of construction. U must be less than or equal to 1.0.

To evaluate the cumulative damage factor, a conservative model of a portion of the spent fuel rack in the vicinity of a support pedestal is constructed. Using the archived results of the spent fuel rack dynamic analyses (pedestal load histories versus time) enables a time-history of stress intensity to be established at the most limiting location. This permits establishing a set of alternating stress intensity ranges versus cycles for an SSE and an OBE event. Based on ASME Code Subsection NF guidelines, the cumulative damage factor (U) is conservatively calculated to be 0.950 due to the combined effect of one SSE and twenty OBE events. This value is below the ASME Code limit of 1.0.

6.10.5 Weld Stresses

Weld locations subjected to significant seismic loading are at the bottom of the rack at the baseplate-to-cell connection, at the pedestal-to-baseplate connection, and at cell-to-cell connections. Bounding values of resultant loads are used to qualify these connections. The paragraphs below summarize each of the weld evaluations. The numerical results are also summarized in Table 6.9.1.

a. Baseplate-to-Cell Welds

The highest predicted weld stress for SSE is calculated from the highest R6 value (provided in 6.10.1 above). The ratio of 2.15 is developed from the differences in material thickness and length versus weld throat dimension and length:

RATIO = ([redacted] in * [redacted] in) / ([redacted] in * 0.7071 * [redacted] in) = 2.15

R6 (obe) * [(0.6) Fy] * RATIO = 0.494 * [0.6 * 21300 psi] * 2.15 = 13,574 psi
R6 (sse) * [(1.2) Fy] * RATIO = 0.443 * [1.2 * 21300 psi] * 2.15 = 24,345 psi

The above calculated values are less than the OBE allowable weld stress value of 19,860 psi and weld stress allowable value of 35,748 psi. Therefore, weld stresses between the baseplate and cell wall base are acceptable.

b. Baseplate-to-Pedestal Welds

The maximum weld stress between the baseplate and the support pedestal, 15,380 psi under an SSE event and 13,600 psi under an OBE event, is verified to be less than the allowable values of 35,748 psi and 19,860 psi, respectively.

c. Cell-to-Cell Welds

Cell-to-cell connections are formed by a series of connecting welds along the cell height. Stresses in storage cell to cell welds develop due to fuel assembly impacts with the cell wall. These weld stresses are conservatively calculated by assuming that fuel assemblies in adjacent cells are moving out of phase with one another so that impact loads in two adjacent cells are in opposite directions; this tends to separate the two cells from each other at the weld.

Table 6.9.1 gives results for the maximum allowable load that can be transferred by these welds based on the available weld area. An upper bound of the transferred load is also given in Table 6.9.1, and it is much lower than the allowable load. This upper bound value is conservatively obtained by applying the maximum rack-to-fuel impact load from any simulation in two orthogonal directions simultaneously and multiplying the result by

2 to account for the simultaneous impact of two assemblies. An equilibrium analysis at the connection then yields an upper bound of the transferred load. It is seen from the result in Table 6.9.1 that the calculated load is well below the allowable.

6.11 Level A Evaluation

The Level A condition is not a governing condition for spent fuel racks since the general level of loading is far less than Level B loading. To illustrate this, the heaviest spent fuel rack is considered under the dead weight load. It is shown below that the maximum pedestal load is low and that further stress evaluations are unnecessary.

LEVEL A MAXIMUM PEDESTAL LOAD

Dry Weight of a 14X11 Rack	=	23,679 lbf
Dry Weight of 154 Fuel Assemblies	=	246,400 lbf
Total Dry Weight	=	270,079 lbf
Total Buoyant Weight (0.87 X Total Dry Weight)	=	234,969 lbf
Load per Pedestal	=	58,742 lbf

The stress allowables for the normal condition is the same as for the upset condition, which resulted in a maximum pedestal load of 144,000 lbs. Since this load (and the corresponding stress throughout the rack members) is greater than the 58,742 lb load calculated above, the seismic condition controls over normal (Gravity) condition.

6.12 Hydrodynamic Loads on Pool Walls

The maximum hydrodynamic pressure (in psi) that develop between the fuel racks and the spent fuel pool walls correspond to the case in which the racks exhibit the largest displacements. The maximum pressure is computed for both the SSE and OBE cases. The results for these worst case conditions are shown in the table below.

Case	Maximum Pressure (psi)
SSE	10.5
OBE	7.5

These hydrodynamic pressures must be considered in the evaluation of the Spent Fuel Pool structure.

6.13 Thermal Stresses From Asymmetric Heat Generation

Inter-cell welded joints are examined under the loading conditions arising from thermal effects due to an isolated hot cell. A thermal gradient between cells will develop when an isolated storage location contains a fuel assembly emitting maximum postulated heat, while the surrounding locations are empty. The temperature difference between these cells can be obtained from section 5.8.3 of this report. The maximum temperature difference between the local water temperature and the bulk SFP temperature is 38.3° F.

We can obtain a conservative estimate of weld stresses along the length of an isolated heated cell by using a finite element model (illustrated in figure 6.13.1) which is based on the following assumptions:

(a) The cell walls surrounding the "hot" cell are assumed to be at the exit temperature of the coolant. In actuality, the water temperature rises monotonically from the bulk temperature value at the base plate elevation to its maximum value at exit. By assuming the cell wall to be at exit temperature of water, the state of computed thermal stress will be maximized.

(b) The cell walls contiguous to the hot cell are assumed to be at the pool bulk temperature.

(c) The connectivity between adjacent cells is through six discrete lineal welds which is explicitly modeled in the finite element model.

(d) The bottom edges of all cell walls are assumed to be fixed.

(e) The top edges of all cell walls are assumed to be free.

The finite element solution exploits the symmetry of the problem about the two vertical planes to permit a quarter symmetric model (figure 6.13.1). It is clear from the physics of the problem and from the above finite element model that the locations of sharp temperature change, namely the longitudinal welds, are locations of maximum stress which arise from restraint of thermal expansion between adjoining cells.

The finite element solution confirms this expected result. The maximum weld shear stress, however, is limited to 8,384 psi. Thermal stresses, which are "secondary stresses" in the stress hierarchy of the ASME Code, have no prescribed limit for NF Class 3 structures. Since the maximum shear stress in weld material is less than the code allowable limit of 19,860 (Table 6.9.1), it is concluded that the "isolated cell" scenario will not lead to any primary yielding in the cell connectivity.

6.14 Overhead Storage

The spent fuel racks for Byron and Braidwood are also qualified for two additional storage functions.

The Region II racks are designed to accommodate an Overhead Platform, which has a capacity of 3 tons (dry). The platform is movable, and it can be installed on top of any Region II rack by inserting its four support legs into empty storage cells. The surface of the platform is elevated 13 inches above the top of the rack and measures 52 inches square, which covers a six by six area of cells. Multiple items can be stored on the platform as long as (i) the total dry weight is less than 6,000 lb and (ii) each item completely rests on the storage surface (i.e., 52 inch square area). The stored objects are protected from falling off of the platform by 14 inch high side walls.

Both the Region I and Region II racks, when they are completely empty, are also capable of supporting miscellaneous equipment (e.g., tools) directly on top of the storage cells. The object must weigh less than 2,000 lb (dry), and it must span a minimum of three storage cells.

6.15 Conclusion

Thirty discrete freestanding dynamic simulations of maximum density spent fuel storage racks have been performed to establish the structural margins of safety. Of the thirty parametric analyses, six simulations consisted of modeling all 24 fuel racks in the pool in one comprehensive Whole Pool Multi Rack (WPMR) model. The remaining twenty-six runs were carried out with the classical single rack 3-D model. The parameters varied in the different runs consisted of the rack/pool liner interface coefficient of friction, extent of storage locations occupied by spent nuclear fuel (ranging from nearly empty to full) and the type of seismic input (SSE or OBE). Maximum (maximum in time and space) values of pedestal vertical, shear forces,

displacements and stress factors (normalized stresses for NF Class 3 linear type structures) have been post-processed from the array of runs and summarized in tables in this chapter. The results show that:

(i) All stresses are well below their corresponding "NF" limits.

(ii) There is no rack-to-rack or rack-to-wall impact anywhere in the cellular region of the rack modules

(iii) The factor of safety against overturning of a rack is in excess of 60.

An evaluation of the fatigue expenditure in the most stressed location in the most heavily loaded rack module under the combined effect of one SSE and twenty OBE events shows that the Cumulative Damage Factor (using Miner's rule) is 0.950, which is less than the permissible value of 1.0.

An evaluation of the thermal (secondary) stress produced by the condition of maximum thermal gradient (obtained when a maximum heat emitting fuel assembly is stored in a cell surrounded by empty storage locations wherein no heat is generated) was performed. The thermal stresses for which no statutory limit in the code (Section III, Subsection NF, Class 3 Structures) exists, is found to be limited to 8,384 psi, which is well below the allowable limit of 19,860 psi.

In conclusion, all evaluations of structural safety, mandated by the OT Position Paper [6.1.2] and the contemporary fuel rack structural analysis practice have been carried out. They demonstrate consistently large margins of safety in all new storage modules.

As a final note, the continued compliance of the installed rack arrays with the licensing basis is an essential part of a plant's safety considerations. Since the fuel racks are free-standing structures, the inter-body spacings in the Byron and Braidwood pools, after a site seismic event, may be different from the as-installed values. A plant's procedures would require a comprehensive survey of the inter-module and module-to-wall gaps subsequent to a seismic event. If the gaps are found to have changed, then a re-evaluation of the acceptability of the module layout configuration (using the WPMR model) will be performed to complete a no-significant-hazards evaluation pursuant to 10CFR50.59. The rack modules will be restored to their original installed locations (pre-seismic) if the conclusion of the §50.59 evaluation is non-

affirmative, or if the plant elects to skip the analytical evaluation (§50.59) step and move directly to reposition the modules.

6.16 References for Section 6

[6.1.1] USNRC NUREG-0800, Standard Review Plan, June 1987.

[6.1.2] (USNRC Office of Technology) "OT Position for Review and Acceptance of Spent Fuel Storage and Handling Applications", dated April 14, 1978, and January 18, 1979 amendment thereto.

[6.2.1] Soler, A.I. and Singh, K.P., "Seismic Responses of Free Standing Fuel Rack Constructions to 3-D Motions", Nuclear Engineering and Design, Vol. 80, pp. 315-329 (1984).

[6.2.2] Soler, A.I. and Singh, K.P., "Some Results from Simultaneous Seismic Simulations of All Racks in a Fuel Pool", INNM Spent Fuel Management Seminar X, January, 1993.

[6.2.3] Singh, K.P. and Soler, A.I., "Seismic Qualification of Free Standing Nuclear Fuel Storage Racks - the Chin Shan Experience, Nuclear Engineering International, UK (March 1991).

[6.2.4] Holtec Proprietary Report HI-961465 - WPMR Analysis User Manual for Pre&Post Processors & Solver, August, 1997.

[6.2.5] Holtec Proprietary Report HI-91700 – Validation Manual for DYNARACK.

[6.4.1] USNRC Standard Review Plan, NUREG-0800 (Section 3.7.1, Rev. 2, 1989).

[6.4.2] Holtec Proprietary Report HI-89364 - Verification and User's Manual for Computer Code GENEQ, January, 1990.

[6.5.1] Rabinowicz, E., "Friction Coefficients of Water Lubricated Stainless Steels for a Spent Fuel Rack Facility," MIT, a report for Boston Edison Company, 1976.

[6.5.2] Singh, K.P. and Soler, A.I., "Dynamic Coupling in a Closely Spaced Two-Body System Vibrating in Liquid Medium: The Case of Fuel Racks," 3rd International Conference on Nuclear Power Safety, Keswick, England, May 1982.

[6.5.3] Fritz, R.J., "The Effects of Liquids on the Dynamic Motions of Immersed Solids," Journal of Engineering for Industry, Trans. of the ASME, February 1972, pp 167-172.

[6.6.1] Levy, S. and Wilkinson, J.P.D., "The Component Element Method in Dynamics with Application to Earthquake and Vehicle Engineering," McGraw Hill, 1976.

[6.6.2] Paul, B., "Fluid Coupling in Fuel Racks: Correlation of Theory and Experiment", (Proprietary), NUSCO/Holtec Report HI-88243.

[6.7.1] ASME Boiler & Pressure Vessel Code, Section III, Subsection NF, 1989 Edition.

[6.7.2] ASME Boiler & Pressure Vessel Code, Section III, Appendices, 1989 Edition.

[6.7.3] USNRC Standard Review Plan, NUREG-0800 (Section 3.8.4, Rev. 2, 1989).

[6.10.1] Chun, R., Witte, M. and Schwartz, M., "Dynamic Impact Effects on Spent Fuel Assemblies," UCID-21246, Lawrence Livermore National Laboratory, October 1987.

HOLTEC INTERNATIONAL

Holtec Center, 555 Lincoln Drive West, Marlton, NJ 08053
Telephone (609) 797-0900
Fax (609) 797-0909

LICENSING REPORT

for

SPENT FUEL RACK INSTALLATION

at

BYRON AND BRAIDWOOD NUCLEAR STATIONS

Holtec Report HI-982083 (Non-Proprietary Version)
Report Category: A

Prepared for Commonwealth Edison Co.
Purchase Order No. 367585
Holtec Project 80944

REVIEW AND CERTIFICATION LOG FOR MULTIPLE AUTHOR DOCUMENTS†

REPORT NUMBER: HI-982083 PROJECT NUMBER: 80944 REPORT TYPE: TECHNICAL REPORT

No.	Document Portion††	REVISION No. 3		REVISION No. 4		REVISION No. 5	
		Author & Date	Reviewer & Date	Author & Date	Reviewer & Date	Author & Date	Reviewer & Date
1.	Chapter 1	N/A		C. Bullock III C.B. 3/3/99	3-3-99	N/A	N/A
2.	Chapter 2	N/A		N/A		N/A	
3.	Chapter 3	N/A		N/A		N/A	
4.	Chapter 4	N/A		N/A		N/A	
5.	Chapter 5	N/A		C. Bullock III C.B. 3/3/99	3-3-99	N/A	N/A
6.	Chapter 6	N/A		N/A		C. Bullock III C.B. 7/1/99	Scott Pellett SHP 7-1-99
7.	Chapter 7	N/A		N/A		C. Bullock III C.B. 7/1/99	Scott Pellett SHP 7-1-99
8.	Chapter 8	N/A		C. Bullock III C.B. 3/3/99	3-3-99	C. Bullock III CB. 7/1/99	Scott Pellett SHP 7-1-99
P.M. (OR DESIGNEE) & DATE		Carl W. Bullock III 2/22/99		Carl W. Bullock III 3/3/99		C. W. Bullock III 7/1/99.	
QA APPROVAL AND DATE		V. Gupta V. Gupta 2-22-99		V. Gupta V. Gupta 3-3-99		S. J. 7/2/99	

† The associated Design Verification Checklist must be filled out by the author and the reviewer(s), and saved in the company qualify file *before* this log is signed off. Per HQP 3.2, up to two reviewers may be needed for work product which is new or novel for the company.

†† Chapter or section number.

Notes: A revision of this document will be ordered by the Project Manager if any of its contents is materially affected during evolution of the project. The determination as to the need for revision will be made by the Project Manager with oral input from the Project Team. Signatures and printed names are required in the review block.

THE REVISION CONTROL OF THIS DOCUMENT IS BY A "SUMMARY OF REVISIONS LOG" PLACED BEFORE THE TEXT OF THE REPORT. Form: CL3.2.5

REVIEW AND CERTIFICATION LOG FOR MULTIPLE AUTHOR DOCUMENTS†

REPORT NUMBER: 41-982083 PROJECT NUMBER: 80944 REPORT TYPE: TECHNICAL REPORT

No.	Document Portion††	REVISION No. 3		REVISION No. 4		REVISION No. 5	
		Author & Date	Reviewer & Date	Author & Date	Reviewer & Date	Author & Date	Reviewer & Date
9.	Chapter 9	N/A		N/A		N/A	N/A
10.	Chapter 10	N/A		N/A		N/A	N/A
11.	Chapter 11	C. Bullard C.B. 2/22/99	Pankaj Chaudhary PKC 2/22/99	N/A		N/A	N/A
12.	Chapter 12	N/A		N/A		N/A	N/A
P.M. (OR DESIGNEE) & DATE		Carl W. Bullard 2/22/99		Carl W. Bullard 3/3/99		Carl W. Bullard 7/1/99.	
QA APPROVAL AND DATE		V. Gupta 2-22-99 V. Gupta		V. Gupta V. Gupta 3-3-99		S. Shah S.S. 7/21/99	

† The associated Design Verification Checklist must be filled out by the author and the reviewer(s), and saved in the company qualify file *before* this log is signed off. Per HQP 3.2, up to two reviewers may be needed for work product which is new or novel for the company.

†† Chapter or section number.

Notes: A revision of this document will be ordered by the Project Manager if any of its contents is materially affected during evolution of the project. The determination as to the need for revision will be made by the Project Manager with oral input from the Project Team. Signatures and printed names are required in the review block.

THE REVISION CONTROL OF THIS DOCUMENT IS BY A "SUMMARY OF REVISIONS LOG" PLACED BEFORE THE TEXT OF THE REPORT. Form: CL3.2.5

SUMMARY OF REVISIONS

Revision 0: Inititial issue.

Revision 1: Figures 11.1 through 11.13, which showed a preliminary rack change-out sequence, were removed from Chapter 11 (Installation) and the List of Figures. Minor corrections were also made to the Table of Contents.

Revision 2: Text was added to Sections 11.5 and 11.6, which describe the fuel shuffling and the new rack installation. Minor changes were also made to the Table of Contents.

Revision 3: Minor changes were made to Paragraph 11.1 h. (ALARA Procedure), Subsection 11.7.2, and Subsection 11.7.3.

Revision 4: Editorial changes were made on pages 1-1, 5-2, 5-17, 8-7, and 8-11.

Revision 5: Chapter 7 was reorganized to include a section on construction accidents (i.e., rack drop accident). Figure 6.5.1 and Table 8.2 were also corrected. Table 6.5.3 was added to the report. These changes also affected the Table of Contents and the List of Figures.

TABLE OF CONTENTS

TABLE OF CONTENTS

TABLE OF CONTENTS

TABLE OF CONTENTS

TABLE OF CONTENTS

LIST OF FIGURES

LIST OF FIGURES

LIST OF FIGURES

LIST OF FIGURES

$$(m_1 + M_{11})\, X_1 + M_{12}\, X_2 = \text{applied forces on mass } m_1 + O(X_1^2)$$

$$M_{21}\, X_1 + (m_2 + M_{22})\, X_2 = \text{applied forces on mass } m_2 + O(X_2^2)$$

X_1 and X_2 denote absolute accelerations of masses m_1 and m_2, respectively, and the notation $O(X^2)$ denotes nonlinear terms. The hydrodynamic coupling effect is shown to be composed of an added nonlinear term which varies with geometry and a component which varies with the square of velocity. This is easily shown by considering a typical example where fluid coupling plays a significant role. Consider two long beams of length "l" width "h" and a distance "s" apart:

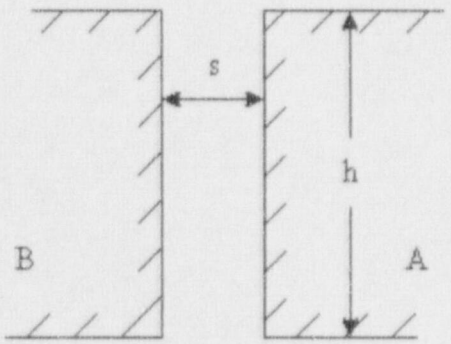

It is assumed that s<<h<<l which is always the case for spent fuel racks. It is shown by Levy [6.6.1] that the force exerted by the fluid on "beam" A is given by

$$F_{opening} = \frac{\rho l h^3}{12 s}\left(-\ddot{s} - \frac{\dot{s}^2}{2s}\right) \qquad \text{(A moves to th right)}$$

$$F_{opening} = \frac{\rho l h^3}{12 s}\left(-\ddot{s} + \frac{\dot{s}^2}{s}\right) \qquad \text{(A moves to the left)}$$

The above solution is valid at each instant in time so that as the beams (racks) approach each other larger forces result which tend to reduce rack motion and preclude rack-to-rack impact. For conservative results, the rack analyses are based only on the nominal gap that exists prior to any seismic event. Therefore the forces exerted have the form.

The analysis for Braidwood serves for Byron as well. In the table, the following coordinate system applies:

x = Horizontal axis along Braidwood plant North (Byron, South)
y = Horizontal axis along Braidwood plant West
z = Vertical axis upward from the rack base

If the simulation model is restricted to two dimensions (one horizontal motion plus one vertical motion, for example), for the purposes of model clarification only, then Figure 6.5.3 describes the configuration. This simpler model is used to elaborate on the various stiffness modeling elements.

Type 3 gap elements modeling impacts between fuel assemblies and racks have local stiffness K_i in Figure 6.5.3. In Table 6.5.2, for example, type 3 gap elements 5 through 8 act on the rattling fuel mass at the rack top. Support pedestal spring rates K_S are modeled by type 3 gap elements 1 through 4, as listed in Table 6.5.2. Local compliance of the concrete floor is included in K_S. The type 2 friction elements listed in Table 6.5.2 are shown in Figure 6.5.3 as K_f. The spring elements depicted in Figure 6.5.4 represent type 1 elements.

Friction at support/liner interface is modeled by the piecewise linear friction springs with suitably large stiffness K_f up to the limiting lateral load :N, where N is the current compression load at the interface between support and liner. At every time-step during transient analysis, the current value of N (either zero if the pedestal has lifted off the liner, or a compressive finite value) is computed.

The gap element K_S, modeling the effective compression stiffness of the structure in the vicinity of the support, includes stiffness of the pedestal, local stiffness of the underlying pool slab, and local stiffness of the rack cellular structure above the pedestal.

The previous discussion is limited to a 2-D model solely for simplicity. Actual analyses incorporate 3-D motions and include all stiffness elements listed in Table 6.5.2. Table 6.5.3 provides a list of typical stiffness values, which are used to model the spent fuel racks for Byron and Braidwood.

a. Baseplate-to-Cell Welds

The highest predicted weld stress for SSE is calculated from the highest R6 value (provided in 6.10.1 above). The ratio of 2.15 is developed from the differences in material thickness and length versus weld throat dimension and length:

RATIO = ([redacted] in * [redacted] in) / ([redacted] in * 0.7071 * [redacted] in) = 2.15

R6 (obe) * [(0.6) Fy] * RATIO = 0.494 * [0.6 * 21300 psi] * 2.15 = 13,574 psi
R6 (sse) * [(1.2) Fy] * RATIO = 0.443 * [1.2 * 21300 psi] * 2.15 = 24,345 psi

The above calculated values are less than the OBE allowable weld stress value of 19,860 psi and weld stress allowable value of 35,748 psi. Therefore, weld stresses between the baseplate and cell wall base are acceptable.

b. Baseplate-to-Pedestal Welds

The maximum weld stress between the baseplate and the support pedestal, 15,380 psi under an SSE event and 13,600 psi under an OBE event, is verified to be less than the allowable values of 35,748 psi and 19,860 psi, respectively.

c. Cell-to-Cell Welds

Cell-to-cell connections are formed by a series of connecting welds along the cell height. Stresses in storage cell to cell welds develop due to fuel assembly impacts with the cell wall. These weld stresses are conservatively calculated by assuming that fuel assemblies in adjacent cells are moving out of phase with one another so that impact loads in two adjacent cells are in opposite directions; this tends to separate the two cells from each other at the weld.

Table 6.9.1 gives results for the maximum allowable load that can be transferred by these welds based on the available weld area. An upper bound of the transferred load is also given in Table 6.9.1, and it is much lower than the allowable load. This upper bound value is conservatively obtained by applying the maximum rack-to-fuel impact load from any simulation in two orthogonal directions simultaneously and multiplying the result by

Table 6.5.3 TYPICAL STIFFNESS VALUES FOR BYRON AND BRAIDWOOD SPENT FUEL RACKS†	
Item	**Stiffness Value**
Pedestal Compression Spring	1.010×10^6 lbf/in
Pedestal/Liner Friction Spring	1.010×10^9 lbf/in
Rack Bending Spring in the X-Z Plane	4.672×10^{10} lbf-in/rad
Rack Bending Spring in the Y-Z Plane	2.458×10^{10} lbf-in/rad
Rack Shear Spring in X Direction	3.315×10^6 lbf/in
Rack Shear Spring in Y Direction	2.775×10^6 lbf/in
Rack Extension Spring	3.298×10^7 lbf/in
Rack Torsional Spring	3.596×10^9 lbf-in/rad
Rack-to-Rack Impact Spring at Baseplate	1.380×10^6 lbf/in
Rack-to-Rack Impact Spring at Top Corner	2.760×10^5 lbf/in

† The values listed correspond to Rack J. The spring constants for other racks vary slightly depending on the shape of the rack and the number of storage cells.

Table 6.9.1

COMPARISON OF BOUNDING CALCULATED LOADS/STRESSES VS CODE ALLOWABLES AT IMPACT LOCATIONS AND WELDS

Item/Location	Calculated	Allowable
Fuel assembly/cell wall impact, lbf	1,148	3,698*
Cell – to – baseplate weld stress, psi	13,574 (OBE) 24,345 (SSE)	19,860 (OBE) 35,748 (SSE)
Pedestal – to – baseplate weld stress, psi	15,380 (SSE) 13,600 (OBE)	35,748 (SSE) 19,860 (OBE)
Cell – to – cell weld load, lbf	15,680** (SSE)	35,748 (SSE)
Maximum rack rotation, degrees	0.478	29.21

* Based on the limit load for a cell wall. The allowable load on the fuel assembly itself may be less than this value but is greater than 1,148 lbs.

** Based on the fuel assembly to cell wall impact load simultaneously applied in two orthogonal directions.

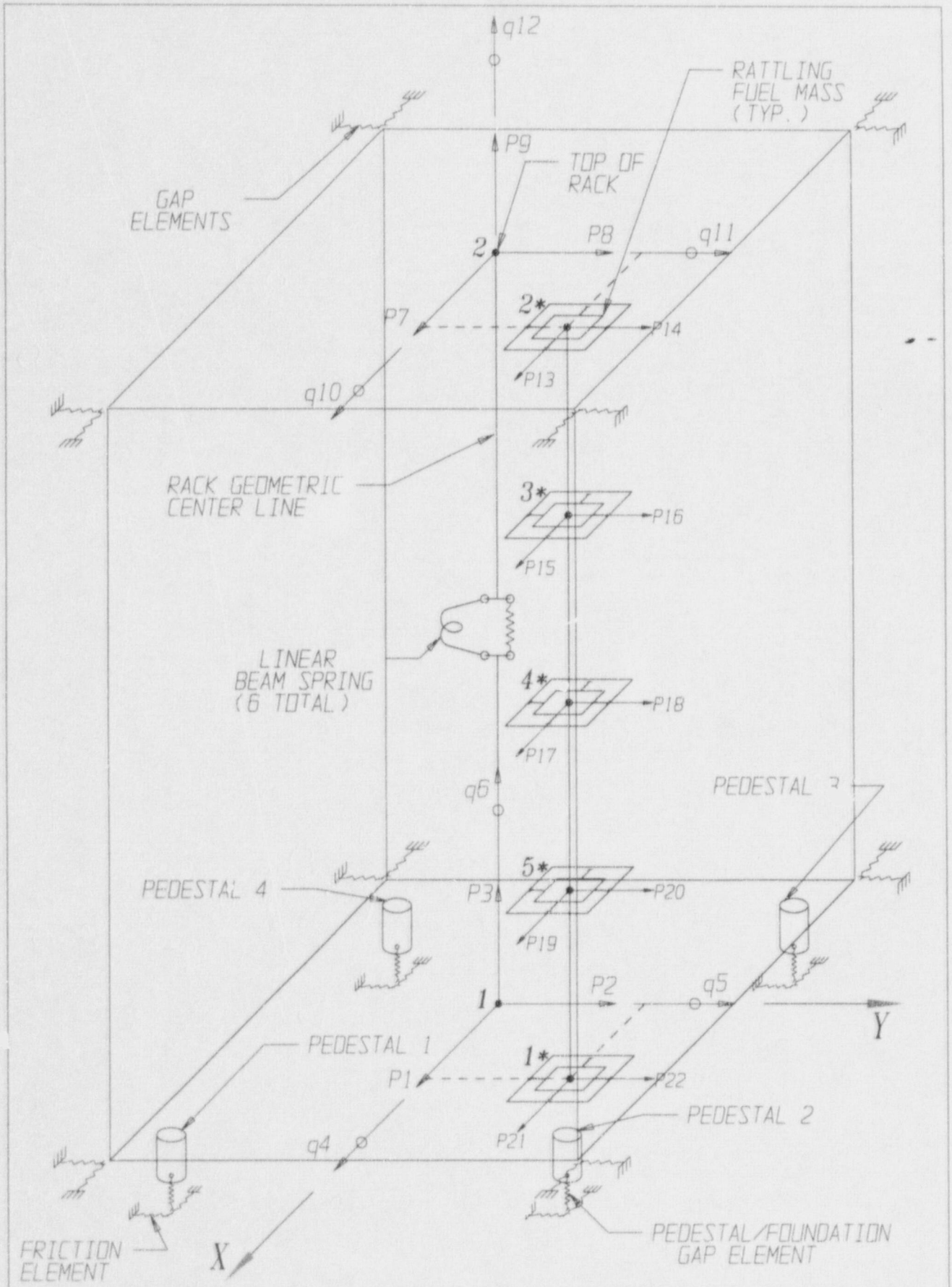

FIGURE 6.5.1; SCHEMATIC OF THE DYNAMIC MODEL OF A SINGLE RACK MODULE USED IN DYNARACK

7.0 FUEL HANDLING AND CONSTRUCTION ACCIDENTS

7.1 Introduction

The USNRC OT position paper [7.1] specifies that the design of the rack must ensure the functional integrity of the spent fuel racks under all credible fuel assembly drop events.

This chapter contains synopses of the analyses carried out to demonstrate the regulatory compliance of the proposed racks under postulated fuel assembly drop scenarios germane to the fuel pools. A potential rack drop accident is also considered in Section 7.3.

7.2 Fuel Handling Accidents

7.2.1 Description

Two categories of fuel assembly accidental drop events are considered. In the so-called "shallow drop" event, a fuel assembly, along with the portion of handling tool, which is severable in the case of a single element failure, is assumed to drop vertically and hit the top of the rack. The damage due to a perfectly vertical drop, on the top of a rack, bounds an inclined fuel assembly drop because the impact energy is focused on a single cell wall, which results in maximum cell blockage. For thermal hydraulic considerations, the maximum cell blockage is conservatively applied to every rack cell Inasmuch as the new racks are of honeycomb construction, the deformation produced by the impact is expected to be confined to the region of collision. However, the "depth" of damage to the affected cell walls must be demonstrated to remain limited to the portion of the cell above the top of the "active fuel region", which is essentially the elevation of the top of the Boral neutron absorber. Stated in qualitative terms, this criterion implies that the plastic deformation of the rack cell walls should not extend more than 17 inches (downwards) from the top. In order to utilize an upper bound of kinetic energy at impact, the impactor is assumed to weigh 2,300 lbs and the free-fall height is assumed to be 36 inches.

It is readily apparent from the description of the rack modules in Section 3 that the impact resistance of a rack at its periphery is considerably less than its interior. Accordingly, the limiting shallow drop scenario, which would produce maximum cell wall deformation, consists of the case where the fuel assembly impacts the peripheral cell wall.

The second class of "fuel drop event" postulates that the impactor falls through an empty storage cell impacting the rack baseplate. This so-called "deep drop" scenario threatens the structural integrity of the baseplate. If the baseplate is pierced, then the fuel assembly might damage the pool liner (which at 3/16" is considerably thinner) and create an abnormal condition of the enriched zone of fuel assembly outside the "poisoned" space of the fuel rack. To preclude damage to the pool liner and to avoid the potential of an abnormal fuel storage configuration in the aftermath of a deep drop event, it is required that the baseplate remain unpierced and that the maximum lowering of the fuel assembly support surface does not violate subcriticality.

The deep drop event can be classified into two scenarios, namely, drop through a cell located above a support leg (Figure 7.2.2), and drop in an interior cell away from the support pedestal (Figure 7.2.3).

In the first deep drop scenario (Figure 7.2.2), the baseplate is buttressed by the support pedestal and presents a hardened impact surface, resulting in a high load. The principal design objective is to ensure that the support pedestal does not tear the liner that overlays the reinforced concrete pool slab.

In the second deep drop scenario (Figure 7.2.3), the fuel assembly impacts the baseplate away from the support pedestals, where it is more flexible. Severing and large deflection of the baseplate leading to a potential secondary impact with the pool liner are unacceptable results.

7.2.2 Incident Fuel Assembly Velocity

Fuel assembly drop events fall into two broad categories of underwater motion, which may be denoted as "geometry unconstrained" (GU) and "geometry constrained" (GC). In the shallow drop scenario, the fuel assembly, which falls from 36" above the rack and is accelerated by gravity, is solely opposed by the force arising from the form drag effect of the unconfined body of water. In this case the Newtonian equation of motion has the form:

$$(m + m_H)\ddot{x} = mg - \frac{C_D A \rho \dot{x}^2}{2}$$

where:

m:	mass of the impactor
m_H:	hydrodynamic (virtual) mass (due to submergence)
x:	displacement variable
g:	acceleration due to gravity
c_D:	form drag coefficient
A:	area subject to drag forces
ρ:	mass density of water
• (dot):	derivative with time
τ:	time coordinate

For a drop from 36" height, the initial conditions are:

$\tau = 0, \dot{x} = 0, x = 0$

The above nonlinear second order differential equation is readily solved to obtain the incident impact velocity (i.e., $\dot{x}$ at $x = 36$ inches).

The geometry constrained (GC) drop scenario corresponds to the downward movement of the fuel assembly through a storage cell. In this case, a portion of the linear momentum of the fuel assembly is absorbed by the water, which is displaced by the movement of the fuel and forced to exit through the opening in the baseplate. Additional dissipation of the fuel assembly's kinetic energy occurs through the forced flow of water into the wake of the advancing fuel assembly. The equation of motion for this case has the form:

$$(m + m_H)\ddot{x} = mg - f(x, \dot{x}, d_1, d_2)$$

where the term f is the fluid resistive force at time τ, which is a function of the coincident axial location of the fuel assembly, x, its velocity, $\dot{x}$, size of the bottom opening in the baseplate, d_1, and the size of the top opening in the storage cell, d_2. The constrained geometry equation of motion is also a nonlinear second order differential equation which can be numerically integrated to determine the incident velocity of the impactor at the instant of its collision with the baseplate.

7.2.3 Mathematical Model

In the first step of the solution process, the velocity of the dropped object (impactor) is computed for the condition of underwater free fall in the manner of the formulation presented in the above section. Table 7.1 contains the results of the three drop events.

In the second step of the solution, an elasto-plastic finite element model of the impacted region on Holtec's computer Code PLASTIPACT (Los Alamos Laboratory's LS-DYNA implemented on Holtec's QA system) is prepared. PLASTIPACT simulates the transient collision event with full consideration of plastic, large deformation, wave propagation, and elastic/plastic buckling modes. The impactor (spent fuel assembly) is simulated by an equivalent elasto-plastic lineal element with lumped masses at its two extremities. The physical properties of material types undergoing deformation in the postulated impact events are summarized in Table 7.2

7.2.4 Results

7.2.4.1 Shallow Drop Events

Of the Region I and Region II racks, module M (10x8) is structurally weakest, and it is used in all impact simulations. The location of the target region in the peripheral scenario is shown in a plan view (Figure 7.2.4).

Dynamic analyses show that the top of the impacted region undergoes severe localized deformation. Figure 7.2.5 shows an isometric view of the post-impact geometry of the rack. The maximum depth of plastic deformation is limited to 16 inches, which is below the design limit of 17 inches.

7.2.4.2 Deep Drop Events

The deep drop events wherein the impact region is located above the support pedestal (Figure 7.2.6) is found to produce limited stresses in the liner and the concrete slab. The maximum stresses are well below the failure limits, as shown in Figures 7.2.7 and 7.2.8. Therefore, we conclude that the pool liner and the concrete slab will not be damaged.

The deep drop condition through an interior cell does produce some deformation of the baseplate and localized severing of the baseplate/cell wall welds (Figure 7.2.9). However, the fuel assembly support surface is lowered by a maximum of 1.25 inches, which is much less than the distance of 14 inches from the baseplate to the liner. Therefore, the pool liner will not be damaged.

7.3 Construction Accidents

A construction accident resulting in a rack drop is an extremely unlikely event. Prior to use, the operability of the cranes will be checked, the lift equipment and rigging will be inspected, and the operators of lift equipment and cranes will be trained. Safe load paths will be followed, and Byron and Braidwood Stations' commitments to the provisions of NUREG-0612 will be implemented by use of written procedures, which have been utilized for numerous other similar rack installation projects.

In the unlikely event of a rack drop, a leak chase system located beneath the spent fuel pool liner is capable of collecting and isolating the leakage. A rack drop would present limited structural damage to the spent fuel pool slab because it is founded on rock and soil. Local concrete crushing and possible liner puncture could occur. Failure of the liner would not result in a significant loss of water, and no safety related equipment would be affected by the leakage. Make up water is available from three separate sources. There are two 500,000 gallon Refueling Water Storage Tanks, non-category 1 back up water sources, and the unborated Safety Category 1 fire protection system available for spent fuel pool water make up.

7.4 Conclusion

The fuel assembly drop accident events postulated for the Byron/Braidwood fuel pools were analyzed and found to produce localized damage well within the design limits for the racks. The shallow drop event is found to produce certain plastic deformation in the top of the storage cell, but the region of permanent strain is limited to the portion of the rack structure situated above the top of the active fuel region. The deep drop case analyzed for the scenario to produce maximum pedestal force, indicates that the pedestal axial load is small enough to preclude liner damage. The analysis of the deep drop event at cell locations selected to maximize baseplate deformation indicates that the downward displacement of the baseplate is limited to 1.25 inches, which ensures that a secondary impact of the fuel assembly with the pool liner would not occur. We therefore concluded that the new high-density spent fuel racks for the Byron/Braidwood pools

possess acceptable margins of safety under the mechanical fuel handling accidents postulated in the OT Position Paper [7.1].

Numerous safety measures are in place, which help eliminate the potential for a rack drop accident. Nevertheless, if a rack drop event does occur, the leak chase system and the available make up water can control the postulated damage.

7.5 References for Section 7

[7.1] "OT Position for Review and Acceptance of Spent Fuel Storage and Handling Applications," dated April 14, 1978.

[7.2] "Analysis of the Mechanical Accidents for Byron/Braidwood Nuclear Station," Holtec Report No. HI-982086, Rev. 1.

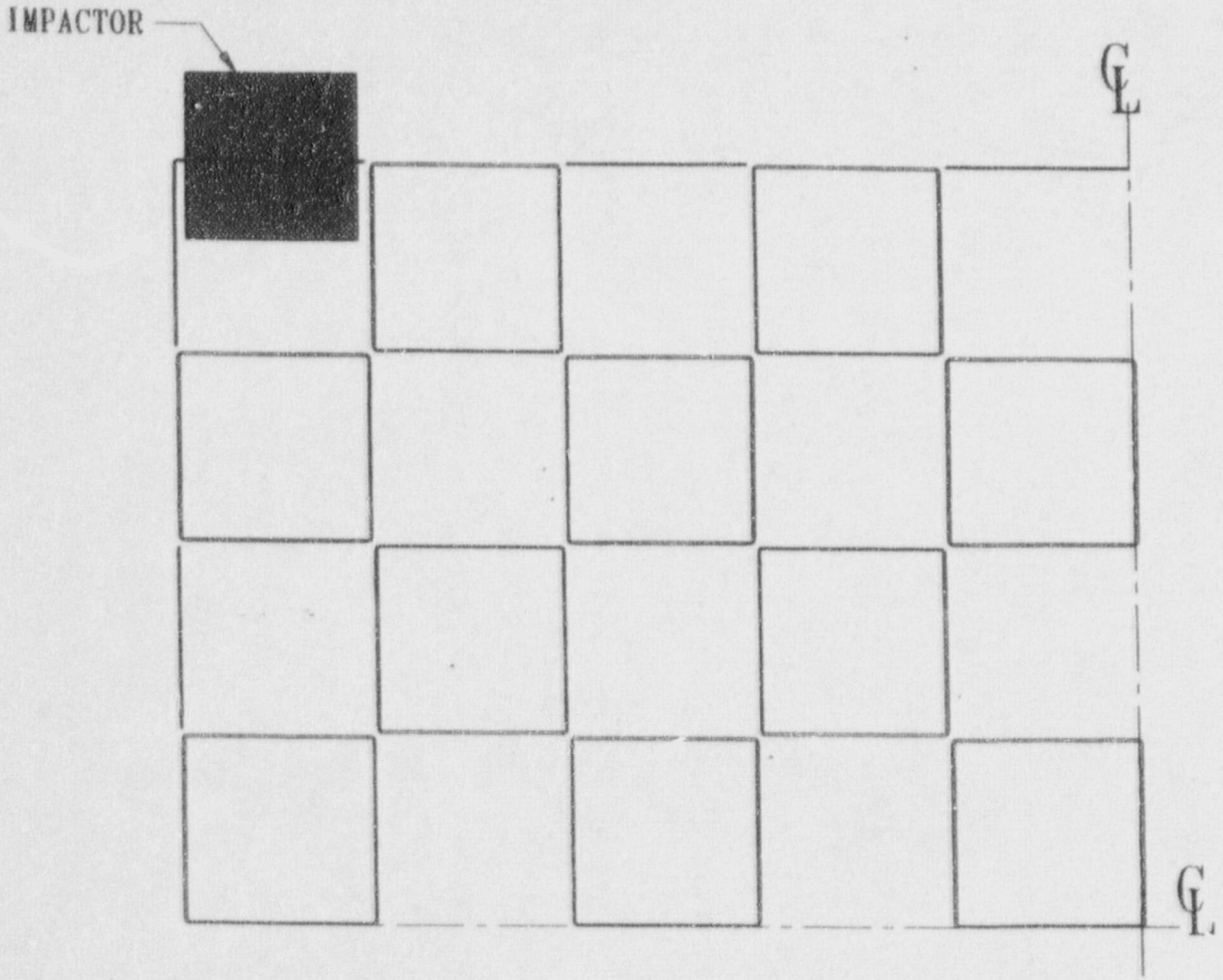

FIGURE 7.2.4 PLAN VIEW OF SHALLOW DROP SCENARIO

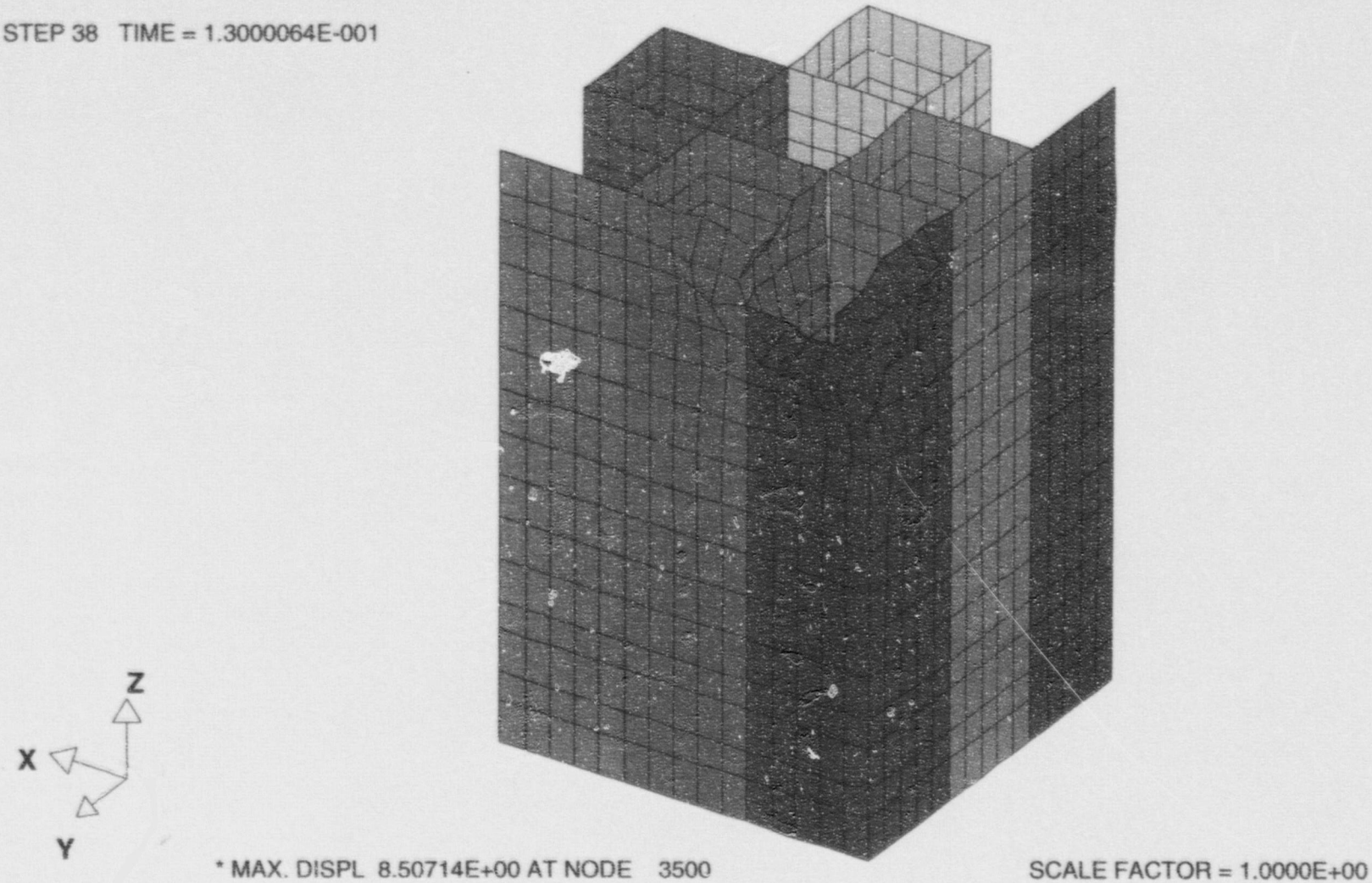

FIGURE 7.2.5 MAXIMUM CELL DEFORMATION FOR SHALLOW DROP

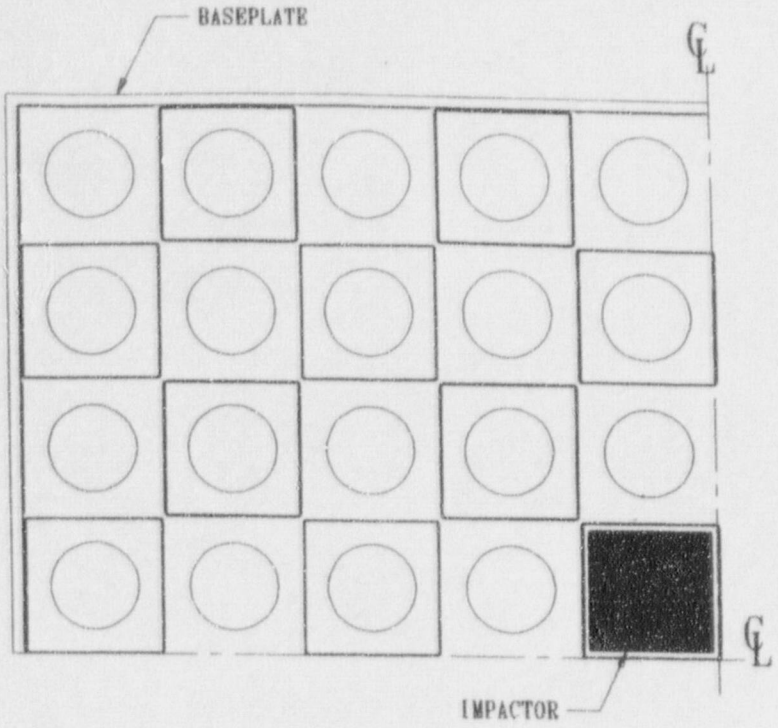

(a) *SCENARIO* SC1

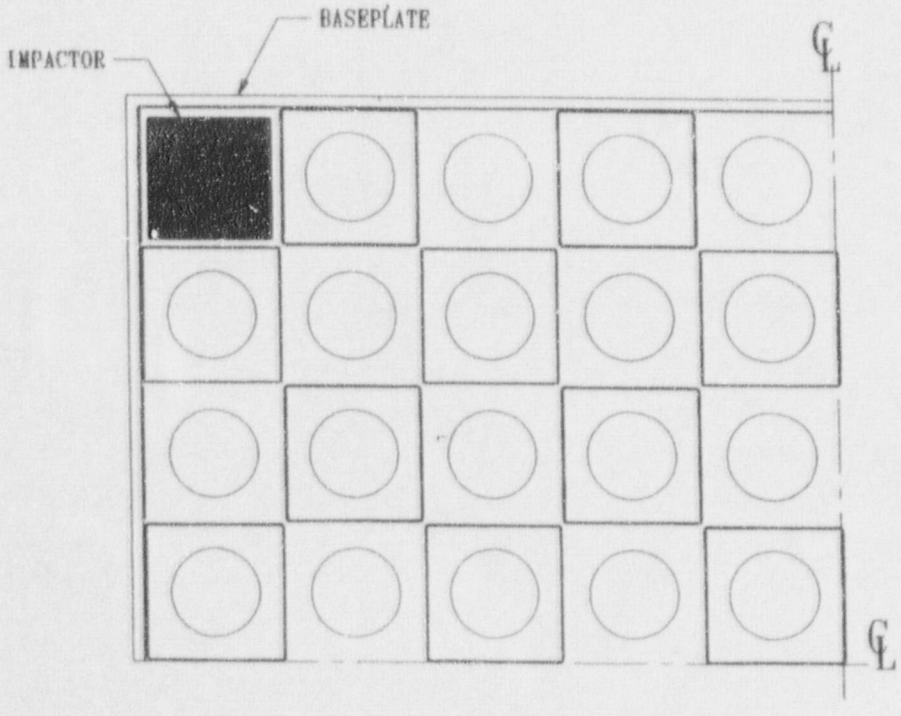

(b) *SCENARIO* SC2

FIGURE 7.2.6 PLAN VIEW OF DEEP DROP SCENARIOS

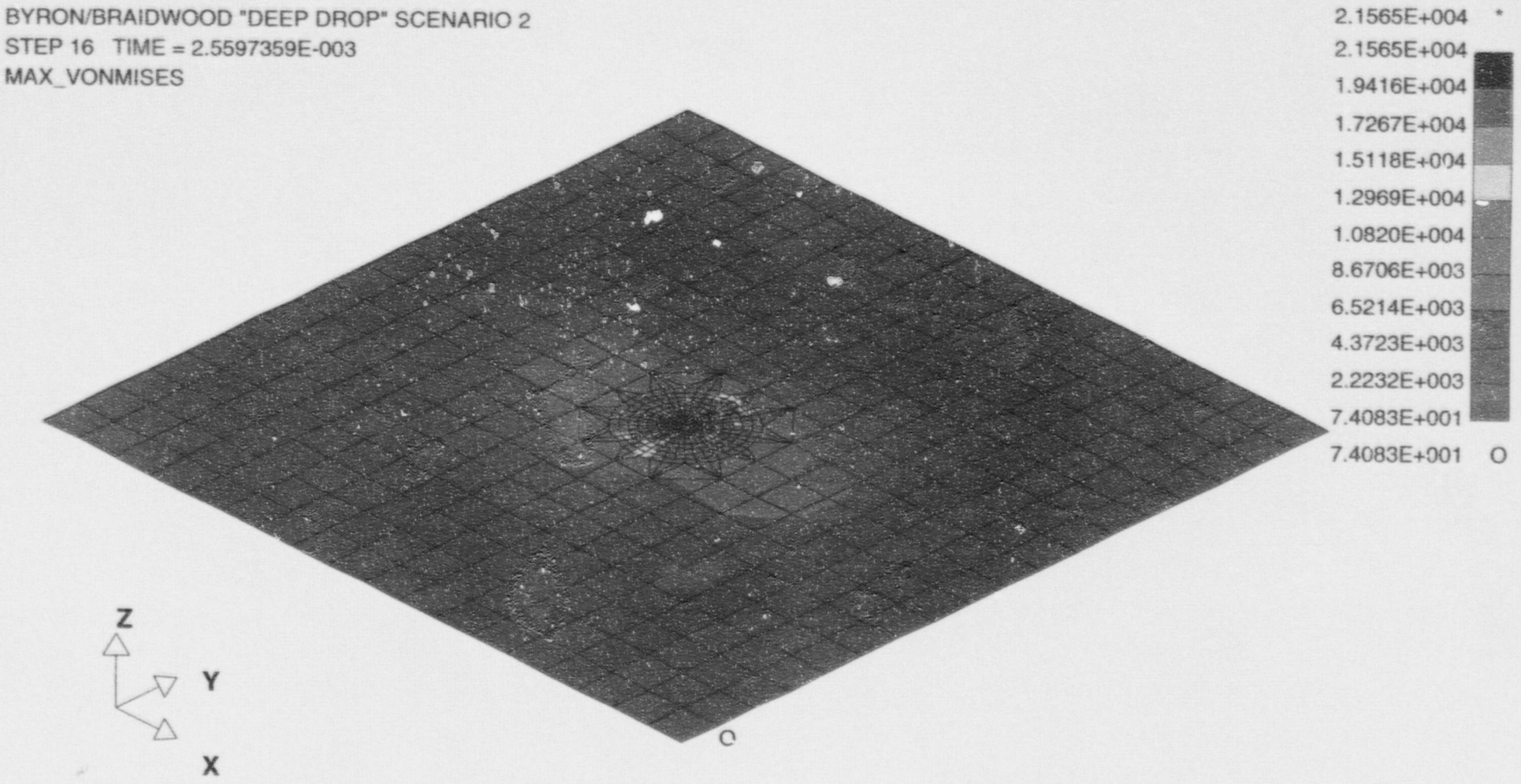

FIGURE 7.2.7 MAXIMUM VON MISES STRESS OF THE LINER FOR DEEP DROP SCENARIO 2

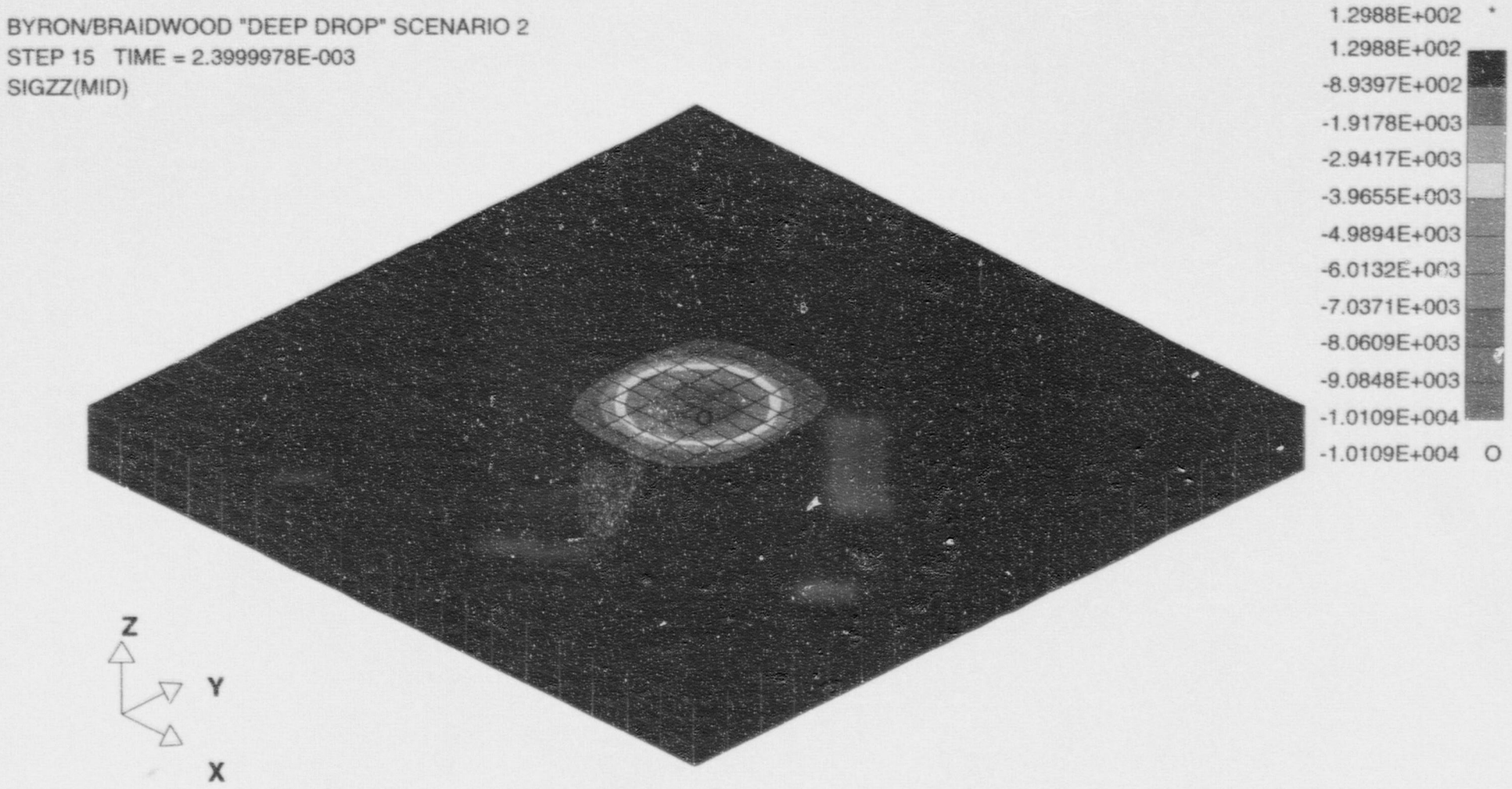

FIGURE 7.2.8 MAXIMUM COMPRESSIVE STRESS OF THE CONCRETE SLAB FOR DEEP DROP SCENARIO SC2

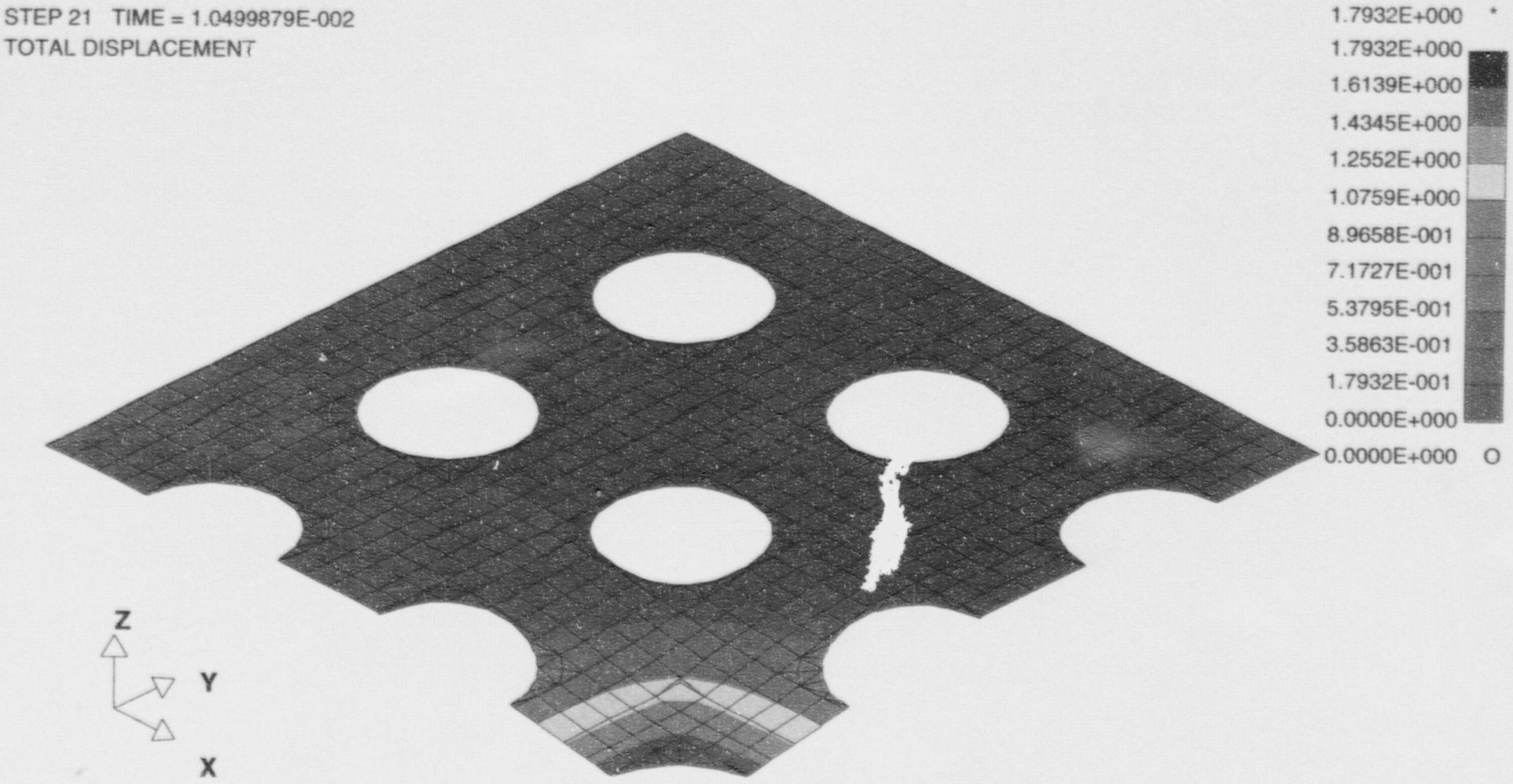

FIGURE 7.2.9 MAXIMUM BASEPLATE DEFORMATION FOR DEEP DROP SCENARIO SC1

Table 8.2.1: BYRON/BRAIDWOOD POOL STRUCTURE DATA

Item	Thickness
Base Mat	6'-0"
North and South Walls	5'-0"
East Wall (Byron) West Wall (Braidwood)	5'-6"
West Wall (Byron) East Wall (Braidwood)	6'-0"
Height (four walls)	41'-0"

8.3 Material Properties

The design basis evaluation [8.1.5] utilized conservative material properties so as to minimize the computed ultimate strength of the pool structure. Table 8.3.1 provides a summary of the key material properties.

Table 8.3.1: MATERIAL PROPERTIES

Parameter	Value
Concrete Compressive Strength (psi)	3.500E+03
Un-Cracked Concrete Elastic Modulus (psi)	3.372E+06
Concrete Poisson's Ratio	0.167
Concrete Weight Density (lb/ft^3)	150.0
Concrete Thermal Expansion Coefficient	5.500E-06
Reinforcement Yield Strength (psi)	6.000E+04
Reinforcement Elastic Modulus (psi)	2.900E+07